# A COMPARISON OF HEMODYNAMIC PERFORMANCE IN MECHANICAL AND BIOLOGICAL HEART VALVE PROSTHESES

by

Philip Mathew

A thesis submitted in partial fulfillment of the requirements for the degree of

M.S. Mechanical Engineering

University of Tennessee at Chattanooga

2010

UNIVERSITY OF TENNESSEE AT CHATTANOOGA

ABSTRACT

A Comparison of Hemodynamic Performance in Mechanical and Biological Heart Valve Prostheses

by Philip Mathew

Chairperson of the Thesis Committee:

Dr. James Hiestand
College of Engineering

Heart valve prostheses are used to replace heart valves in patients afflicted with valvular heart disease. The malfunctioning heart valve adversely affects the fluid mechanical performance. While the choice of mechanical VS biological valve prostheses is dependent on the patient, the biological valves should have improved hemodynamic performance compared to the mechanical valves. This work focused on CFD analysis of the Starr-Edwards caged ball valve and a biological valve and serves to validate the improved hemodynamics of the latter valve in comparison to the former. Commercial CFD software (CFD-GEOM, CFD-ACE, CFD-VIEW) are used for the analysis. The main results are: Smaller pressure drop across the biological valve compared to the Starr-Edwards valve, smaller downstream turbulent kinetic energy production in the biological valve compared to the Starr-Edwards valve, and smaller shear stress associated with the biological valve compared to the Starr-Edwards valve.

TABLE OF CONTENTS

LIST OF FIGURES

# ACKNOWLEDGMENTS

I would like to thank Dr. James Hiestand for his time, patience, honesty, and willingness to serve as my advisor on this project. Over the course of this project, we have shared many jokes and stories. He has not only served as a thesis advisor, but also a source of encouragement. Our discussions (both academic and general) were the epitome of everything I wanted in a graduate education. I would also like to thank Dr. Ron Goulet, Dr. Prakash Damshala, and Dr. Joseph Owino for serving on my thesis committee.

I want to thank the members of my committee for serving as mentors and friends both inside and outside the classroom. Throughout my graduate school experience, I have been treated like a colleague rather than a student and for this, I am extremely grateful and humbled.

Thanks also goes out to Harold Head, M.D. for all his help, expertise, and willingness to help. His many years of experience in the medical field provided valuable insight for this project.

I also want to thank my parents, Sam and Silu, for their support (and for my mom's college anatomy books), my sister, Mayu, for inspiring me to "think outside the box" and to work on something unique, and my beautiful fiancée, Shakila, for her love and for her understanding the demands of a thesis. Last but certainly not least, I thank my nephews, Caleb and Jacob. They showed their support by graciously giving me time off from video game playing and wrestling so I could focus on this project.

# DEDICATION

This work is dedicated to God for His blessings, to my family for their love and support and to the professors who inspired my love for learning

# Chapter 1

# Introduction

Valvular heart disease is a cardiovascular affliction that affects many people worldwide and requires surgical repair or complete valvular replacement in severe cases. A diseased valve adversely affects the hemodynamical performance and often leads to serious medical conditions that are related to the inefficient cardiovascular fluid dynamics. Although heart valves can be replaced through homograft procedures (where a valve is taken from a cadaver), the number of valvular disease cases make the development of functioning prosthetics as a necessity. Artificial heart valve designs have evolved from relatively simple configurations to sophisticated designs. Despite the advancements, artificial heart valves are still considered less than ideal due to the intrinsic difficulty of duplicating the native heart valve in terms of biocompatibility and proper dynamics. Most of the problems associated with prostheses are due to design-dependent fluid mechanics. In order to evaluate the improvements of heart valves, one should compare prostheses in terms of hemodynamic performance. Experimental setups that study the fluid mechanics of artificial heart valves are plausible and have been performed but lack the flexibility of computational fluid dynamical models. Whereas it is difficult to recreate anatomically

accurate experimental models, a CFD model is limited only by the capabilities of the software used and the skills of model's creator. The pulsatile flow through heart valves poses a significant challenge since the details of the dynamics of the valve leaflets as a function of the cardiac cycle should be specified. Due to this difficulty, CFD models of heart valves (both natural and prosthestic) often are modeled as steady-state with specified parameters (such as pressure and inlet velocity). This approach requires a knowledge of the valve's location relative the valvular orifice.

With the development of new artificial heart valves, an important question arises from the engineering perspective: Have the modern biological models shown any significant hemodynamical improvement over the mechanical models? Significant advancements in terms of functional hemodynamics would allow for attention to be focused on other aspects of prosthesis development such as biocompatibility[1] and delivery methods. A lack of any improvement gives the impression the entire endeavour might be seen as futile effort.

This work addresses the issue of improved hemodynamics of the aortic prosthesis by using commercial CFD software (CFD-GEOM, CFD-ACE, CFD-VIEW[2]) to validate the improved hemodynamic performance of a modern biological valve compared to the Starr-Edwards (SE) caged ball valve. Effort is focused on evaluating vital variables of interest such as pressure drop, turbulence production, flow patterns, shear stresses, and hemolysis.

[1]While an important issue, biocompatibility will not be discussed in full detail since the focus of this work is on functional hemodynamics.

[2]All software mentioned were developed by the ESI Group.

# Chapter 2

# Heart Valve Anatomy and Function

The tissues of the human body rely on a constant supply of oxygen and nutrients that are provided by blood circulation. The heart is the bio-mechanical pump that sends blood into circulation in three distinct circulatory systems. The systemic system delivers oxygen-rich blood to the organs of the body, the coronary system carries oxygenated blood through the myocardial tissue of the heart itself[1], and the pulmonary system allows for blood to be oxygenated in the lungs. The human heart consists of four chambers (two atria and two ventricles). Each side of the heart contains two chambers (a respective atrium and ventricle) and the sides are divided by a interventricular/interatrial septum (depending on which chambers are being separated). The left and right atria serve as entry-points to the heart and the atria lead into their respective ventricles [1]. A flow schematic of the circulation systems and their relationship to the heart chambers is shown in Fig. 2.1. In order to ensure a one way flow, a system of heart valves open and close in accordance

[1] A separate system for blood circulation is needed for the heart. Despite the fact that the heart is continuously bathed in blood, the blood's time duration in the heart is significantly short (and the myocardium is too thick) to allow direct diffusion.

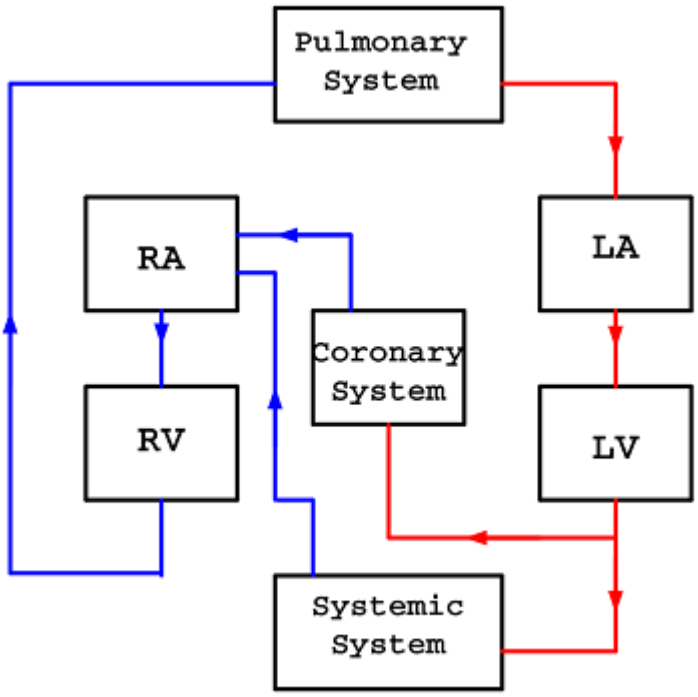


Figure 2.1: **Simplified Flow Schematic of Human Circulatory System**: LA denotes the left atrium, RA denotes the right atrium, LV denotes the left ventricle, RV denotes the right ventricle. The red line leaving the pulmonary system represents oxygenated blood while the blue lines leaving the systemic and coronary systems represent deoxygenated blood flow.

to oscillatory flow at the atrio-ventricular and ventricular-outflow junctions[2]. As opposed to the cardiovascular contraction-relaxation mechanisms which rely on an intrinsic electrical system , the heart valves function in a purely mechanical basis by means of cyclic pressure changes due to systole-diastole phases of the cardiac cycle.

[2]The left ventricle leads to the aorta while the right ventricle leads into the pulmonary trunk

## 2.1 Heart Valve Anatomy

The heart valves are fluidic control devices that act as check valves to prevent bi-directional fluid motion. Without the valves, the heart would compress the blood, pushing the blood both upstream and downstream and the blood would fail to circulate properly. A superior aspect of the heart valves is given in Fig. 2.2.

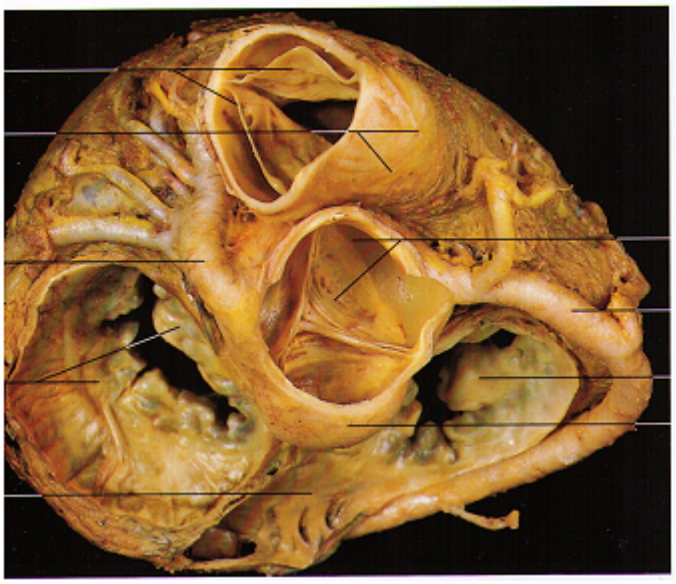

Figure 2.2: **Superior Aspect of Heart Valves:** Image taken from [2] The top valve is the pulmonary semilunar valve which controls blood flow from the right ventricle to the pulmonary arteries. The central valve is the aortic semilunar valve which controls blood flow from the left ventricle to the aorta. The right valve is the tricuspid atrioventricular valve which controls blood flow from the right atrium to the right ventricle. The left valve is the mitral (or bicuspid) valve which controls blood flow from the left atrium to the left ventricle. Note the sinuses of Valsalva and coronary outlets adjacent to the aortic valve.

### 2.1.1 The Atrioventricular Valves

Blood enters the heart through the atria[3] and flows through the atrioventricular junctions that connect the atria to their respective ventricles. During ventricular systole, it is important to obtain high enough ventricular pressure to provide impetus for blood flow. A heart valve with sufficient closure dynamics would be required at the atrio-ventricular junction in order to maintain a high enough pressure for blood flow. For each atrium-ventricle pair, there corresponds an aptly named atrioventricular (AV) valve. The left AV valve is the mitral valve and the right AV valve is the tricuspid valve. The AV valve consists of a four elements:

- The valve annulus
- The valve leaflets
- The chordae tendineae
- The papillary muscles

The valve annulus is composed of a dense ring of tissue enveloped by muscle and the leaflets are composed of endothelium and collagen. The leaflets of the valves are designated by their position but due to the oblique positioning of the valve, neither mitral leaflet can be technically designated as anterior or posterior[4]. The tricuspid valve has three leaflets and the mitral valve has two leaflets[5]. This, along with the location of the AV valve, are the only major differences between the

[3]Oxygen-poor blood coming from the systemic circulatory system enters the right atrium and oxygen-rich blood coming from the pulmonary circulatory system enters the left atrium.

[4]However, the aortic leaflet is often referred to as the anterior leaflet while the longer mural leaflet is considered as the posterior leaflet.

[5]For this reason, the mitral valve is also called the bicuspid valve.

valves since they are biologically and structurally similar. The leaflets are connected to a valve annulus located at the atrioventricular junction. In order to prevent valve prolapse, the leaftlets are provided structural support by chordae tendineae and papillary muscles, which are stalk-like projections protruding from the ventricular walls. A figure showing these anatomical features is given in Fig. 2.3.

### 2.1.2 The Semilunar Valves

The semilunar (SL) valves are located at the ventricle-outflow junction and are similar to the AV valves for their common objective of allowing the ventricle to generate enough internal pressure for blood flow. The left SL valve is the aortic valve and the right SL valve is the pulmonary valve. Like the AV valves, the SL valves are composed of partitioned fibrous leaflets. The aortic valve is situated in the aortic root, which represents the outflow tract and forms a structural support for the leaflets [3]. Superior to the leaflets are the sinuses which contain the inlets into the coronary system. The sinuses are anatomically a part of the sinotubular junction. In the human aortic valve, the SL leaflet is attached to the vessel wall at the basal attachment. The proximal points of attachment for each leaflet form a commissure and the free edges of the leaflets coapt to prevent regurgitant flow during valve closure. Functionally, the three sinuses of the aortic root and their respective leaflets are similar but there are anatomic distinctions since two of the sinuses possess coronary inlets while the third (the aptly named non-coronary sinus) does not. It has been suspected that vortices formed in the sinuses aid in closure dynamics by creating transverse pressure gradients to force the leaflets closed [4].

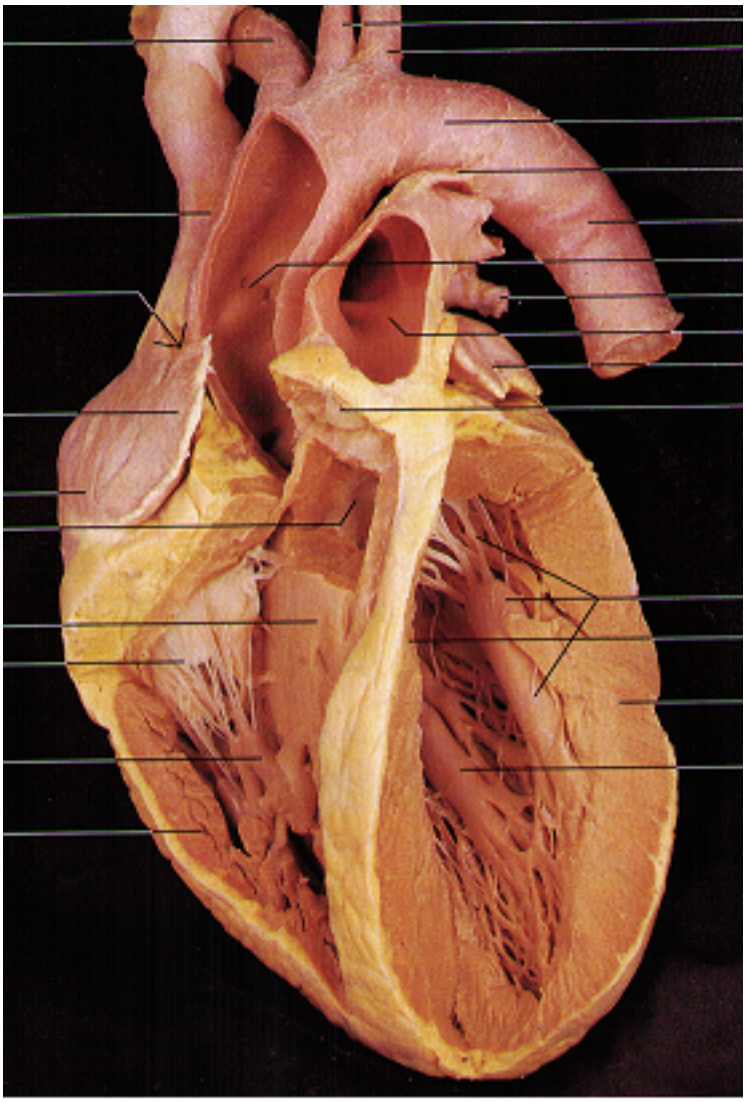

Figure 2.3: **Anterior Aspect of Open Heart:** Image taken from [2]. The papillary muscles are shown to project from the ventricle wall and are connected to the atrioventricular valves by the chordae tendineae (the string-like structure which resembles the cables of a parachute). The mitral valve (on the right) is slightly obscured by the septum. Note the thickness of the myocardium on the heart's left side compared to the right side (this is due to the higher pressure associated with the left side of the heart).

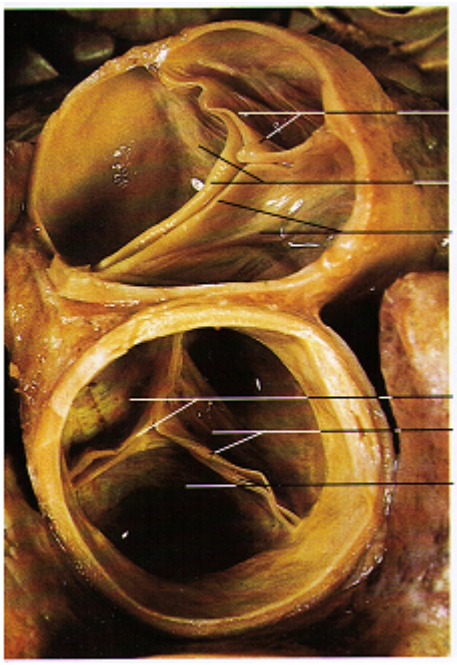

Figure 2.4: **Superior Aspect of Semilunar Valves:** Image taken from [2]. The pulmonary valve (above) and the aortic valve (below). Both valves are depicted as closed and the coaptation region (lunula) is shown projecting outward.

The leaflet of the SL valve is a composite layering of endothelial cells, ventricularis, spongiosa, and fibrosa [4]. The leaflet surface adjacent to the aorta is the fibrosa. A thinner layer of collagen and elastin (the ventricularis) is located on the side of the leaflet that is adjacent to the ventricle. As the ventricularis is the primary layer in contact with the blood flow during ventricular systole, it is a smooth surface to allow less resistance to blood flow. The central portion of the leaflet is the spongiosa. The spongiosa contributes much to the thickness of the native aortic valve leaflet but does not involve itself with the direct transmission of stress [5]. As a result, modeling the leaflet architecture and its mechanical behavior with response to the cardiac cycle remains a significant challenge.

# Chapter 3

# Artificial Heart Valves

Like any engineering system, the heart cannot be flawless indefinitely and, like any biological system, is susceptible pathological conditions that affect its efficiency.

Heart valve disease is the cardiovascular affliction, infective or non-infective, that adversely affects the functionality of heart valves, often resulting in poor hemodynamic performance. Disorders of the heart valves can be congenital or acquired. Congenital heart valve disorders exist at birth while acquired heart valve disease occurs either by infection or by natural aging. The sources of infection often include rheumatic fever or infective endocarditis. In addition to calcification of the heart valves, myxomatous degeneration is responsible to improper heart valve function. The disease is an affliction of the elderly and is the result of metabolic changes in which the leaflet tissue loses elasticity and develops a starch build-up.

In either case (and particular for acquired heart valve disease), the implementation of artificial heart valves has helped many lives but the inability to simulate natural heart valve dynamics has led to complications that are hemodynamical by

nature.

There are two primary valve defects that concern physicians. In stenosis, the leaflets thicken and narrow. This rigidity inhibits proper valve dynamics, thus narrowing the valve and resulting in a greater pressure drop. Stenosis, according to [1], can be congenital but is also associated with scar tissue formation as a result of endocarditis or rheumatic fever. Stenosis, from a hemodynamical perspective, can lead to unfavorable conditions in the downstream environment.

Incompetence is defined as the inability of heart valves to provide adequate closure, thus leading to regurgitation (retrograde blood flow). Although some regurgitant volume is considered acceptable, a significant amount of regurgitant blood flow serves as a clinical red flag, often indicating an intrinsic defect of the heart valve itself (non-invasive methods of determining a potential heart valve defect include listening for murmurs). In an incompetent valve, the heart repumps the same regurgitant volume, and the heart, in order to meet the oxygen demands of the body, is forced to pump harder. The heart pumping harder at longer durations of time places more mechanical strain on the heart.

When a valve's functioning is impaired (be it congenital or acquired), two primary options are considered: heart valve repair or heart valve replacement. A repairing of the defective heart valve is often favored over complete heart valve replacement and the repair can be a matter of separating a fused leaftlet, reshaping valvular tissue (via leaflet shaving) for a "tighter close," or appending tissue

to patch leaftlet fissures [6]. For stenosis cases, balloon valvuloplasty remains an option. Balloon valvuloplasty is the medical procedure in which a balloon-tipped catheter is utilized to widen the lumen[1]. It's particularly attractive for cases involving children/infants with congenital conditions of the mitral valve, since the procedure does not affect the growth of the valve and the recovery time is shorter than surgery.

For complete heart valve replacement, the Ross procedure remains one of the more feasible procedures. The Ross procedure involves replacing the faulty aortic valve with the pulmonary valve from the same individual (an autograft procedure) and the pulmonary valve is replaced with a pulmonary valve from a deceased human donor (a homograft). Although replacing the diseased aortic valve with the aortic valve from a deceased human donor seems less tedious, the allografts from cadavers consist of nonliving tissue. This poses a disadvantage since these allografts lack the proper cellular regeneration mechanisms needed for self-repair. As a result, the valve is prone to long-term mechanical wear [4]. Though the Ross procedure is suitable for children and infants since there will be a continued growth of the valve, the procedure is surgically complicated, requiring a tremendous amount of skill and patience on behalf of the surgeon. In addition, the Ross procedure being a more involved and taxing surgical undertaking since it involves a double-valve replacement and allows for greater risk due to complications.

For dilapidated heart valves, a prosthesis can be employed to potentially prolong the lifetime of a patient. Artificial heart valves fall into two broad categories:

[1]The lumen is the central, blood-containing part of the vessel.

mechanical and biological.

## 3.1 A Brief Historical Discussion of Heart Valves

Dr. Charles Hufnagel is credited with the first clinicial use of a prosthesis [7]. The Hufnagel prosthesis consisted of a non-constrained ball occluder placed in a open-ended plexiglass tube. It operated in the same manner as caged-ball valves of today but as opposed to modern aortic artificial valves, Hufnagel's caged ball valve was not placed at the sinotubular junction, but in the descending aorta. In 1960, the Starr-Edwards (SE) caged ball valve was first used in the clinical setting. Using the general configuration of the Hufnagel setup, the SE valve used a ball occluder in a cage but unlike the Hufnagel prosthesis, the SE valve was placed in the anatomic location. As with any engineering device, steps were taken to improve the mechanical and fluid dynamical performance of the caged-ball valve. The caged-ball valve evolved into various designs including the DeBakey-Surgitool, Smeloff-Cutter, and Magovern-Cromie. Each design implemented new characteristics to improve overall performance. The Smeloff-Cutter mechanical valve employed a Teflon sewing ring, bio-compatible titanium cages, and a smaller silcone-rubber ball to improve hemodynamics . Because of the legitimate concern of the occluder being displaced, the Smeloff-Cutter valve possessed two cages for both sides of the valve orifice. The distinguishing feature of the Smeloff-Cutter valve (its smaller ball occluder size) was also a source of problems. Due to lipid absorption, the ball occluder would swell, sometimes leading to the ball being physically lodged in the orifice. As a result, the valve's use in the clinical setting was discontinued due to potentially life-threatening conditions. The Magovern-Cromie valve followed the general caged-ball design with

an important feature. As opposed to earlier caged-ball valve models, the Magovern-Cromie valve used hooks around the perimeter of the valve's base ring. The surgeon would lower the valve into place and use the angled hooks to anchor the valve. As a result, the Magovern-Cromie valve did not require a sewing ring and was aptly labeled as a sutureless prosthesis. Despite the innovations and the durability of the basic caged-ball valve design, the occluding design results in energy-inefficient hemodynamics, greater pressure drops compared to native heart valves, and higher downstream turbulent stresses.

With the relatively poor hemodynamics of the caged-ball valve design, the leaftlet mechanical valve was created as a potentially suitable alternative. Perhaps the most famous of the leaflet valves is the Bjork-Shiley valve. The standard aortic Bjork-Shiley valve consists of a teflon sewing ring with a carbon pyrolytic disk that opened at 60 degrees relative to the plane of the valve. While the 60 degree opening position was still considered rather obstructive to central flow, it still provided better hemodynamics than the caged-ball design. This was due to its design that modeled the dynamics of an airfoil, thus minimizing the disturbance in the flow. The unfortunate drawback of the leaflet models was the thromobogenic nature of the struts and their proclivity for fracture. In 1998, there was an increased number of fatal fracture reports in the primary clinical trial of the Bjork-Shiley valve [4].

While caged-ball and leaflet valves are still in use, they have drawbacks: poor hemodynamics for the former and fracture-prone struts in the latter. The design for an optimal artificial heart valve stems from a very basic and yet important question:

How can engineers simulate the natural dynamics of heart valves? The mechanical valves (both caged-ball and leaflet) fail to duplicate the energy-efficient flow of the native heart valve and the material used in a mechanical valve could induce thrombosis. A viable option is a biological valve. This includes autografts (such as the Ross procedure where the pulmonary valve replaces the aortic valve in the same individual), homografts (valves from a human donor), or heterografts (valves fashioned from an animal donor, usually bovine or porcine by nature). Compared to mechanical prostheses, biological valves present a closer approximation to the natural heart valve since they possess anatomic similarities in leaflet-design, preserve energy-efficient central flow, and are less thrombogenic.

When the engineering of bioprosthetic valves left very little room for improvement, attention was focused on delivery-methods. Early heart valve replacements involved open heart surgery and increased the chances of post-surgery trauma and complications. The latest development in valve replacement is that of catheter-delivered valve replacement. In this surgical technique, a valve-tipped catheter is used to implant the prosthesis via a transfemoral/transapical delivery[2]. The catheter is then threaded (retrograde) to the anatomical location and expanded into place. The valve itself is composed of porcine aortic leaflet or bovine pericardial tissue that is hand-sewn to a nitinol wireframe [8]. This particular valve remains a particularly attractive option since the valve duplicates native heart valve dynamics and the implantation can be performed on a beating heart without need for a heart-lung machine.

[2]Transfemoral delivery is made through an incision in the femoral artery while a transapical delivery is made through a puncture in the apex.

## 3.2 Assessment of Artificial Heart Valves

Studies of artificial heart valves have shown that the most serious problems with heart valve prostheses include tendency for thrombosis, hemorrhage due to anticoagulant therapy (post-implantation), tissue overgrowth, and infection. To account for these considitions, numerous sources ( [7], [9], [10], [4]) provided criteria for the ideal heart design. The heart valve design should:

- be biologically stable in terms of material biocompatibility
- be structurally stable
- produce minimal pressure drops across the valve
- have relatively small regurgitant volumes
- minimize turbulence
- prevent regions of high shear stresses from forming
- avoid creating regions of stagnation or points of flow separation

All of these requirements fall into three categories: improved hemodynamics, structural stability, and biocompatibility. Sometimes there are no clear distinctions between these categories and this work focuses primarily on hemodynamic efficiency.

The pressure drop across a valve represents energy dissipation and is a measure of how efficient a heart valve is for allowing blood flow across the valvular orifice. The pressure drop should be minimized since it affects diffusion-related oxygen consumption of the myocardium [7]. The impeded flow across a valve will often result in a higher pressure drop and thus valves with relatively "sluggish" flow are considered poorly-designed.

In the native aortic heart valve, retrograde blood flow during ventricular diastole effectively closes the valve leaflets to prevent further backflow into ventricle. The proper closure of the heart valve leaflet is aided by the existence of coaptation regions where adjacent leaflets "fold" to form a surface parallel to the aortic wall. The heart can still function properly with "leaky" valves provided that the condition is not severe [1]. Mechanical heart valves lack this feature and so regurgitant volumes are relatively large in comparison to biological valves (some bileaflet models have regurgitant volumes that can be as high as 10 mL/beat [11]). Regurgitant volumes (which include closing volumes in addition to the leakage volume) are dependent on valve type [7].

Running broad calculation using a dynamic viscosity of $\mu = 0.004\ Pa \cdot s$, a density of $\rho = 1050\ kg/m^3$, and a 1 inch diameter[3], $Re \approx 9000$ (indicating turbulent flow)[4]. Turbulence results from abrupt changes in velocity and abrupt changes in the geometry. Turbulence causes concern for heart valve prosthesis design for two reasons:

[3]All these values were used in the CFD simulations. The density, diameter, and dynamic viscosity were taken from [1].

[4]The hydraulic diameter ($D_h = d$) was used

1. Turbulence is a momentum transfer mechanism and the resulting increase in frictional forces requires increased pumping power by the heart.

2. Turbulence can result in eddies which produce turbulent shear stresses.

Turbulence is addressed in more detail later in this work.

### 3.2.1 The Effective Orifice Area and Performance Index

The effective orifice area (EOA) is a measure of a valve design's ability to utilize its primary orifice area [7] and is provided by the Gorlin equation. Although a useful assessment for all prostheses, the EOA is especially useful for mechanical valves that possess an occluding component since the EOA is a quantitative evaluation of blood flow obstruction. Hemodynamically, a larger EOA results in a smaller pressure drop and this may be tied to smaller shear stresses. Despite advances with echocardiography, the Gorlin equation remains a "gold standard" for heart valve assessment [4].

The EOA measures the ability of a heart valve to utilize the orifice area but considering only the EOA of a heart valve can lead to misinterpretation. Clearly a larger heart valve will have a larger EOA but may impede blood flow more compared to a small valve (depending on the valve design). In this particular case, the EOA is not a sufficient assessment for heart valve performance. This requires a normalization of heart valve size in order to compare all heart valve prostheses on equal basis. In order to do this, the performance index (PI) is defined as the ratio of the EOA to the valve sewing ring area (VSRA). The PI is a quantitative measure of the effectiveness of allowing forward flow and is independent of valve size:

$$PI = \frac{EOA}{VSRA} \tag{3.1}$$

With a cardiac output of 5L/beat, a heart rate of 70 beats per minute, and a 120/80 mmHg aortic pressure gives performance indices of aortic caged ball valve designs that range from 0.30 to 0.35. Aortic leaflet/disk models exhibit a wider range of PI values between 0.40 and 0.80 and for aortic biological valves the PI values can range from 0.30 to 0.65 [11]. These values shouldn't be considered as defining limits for prosthesis PI.

## 3.3 Problems with Prosthetic Heart Valves

Prosthetic heart valves, despite decades of technological advancements, still have problems that prevent them from being acceptable as an ideal heart valve replacement. Major problems associated with the valve-structure and environment interaction often involve material fatigue, infection, and hemorrhage associated with anti-coagulant therapy [7]. Perhaps the most serious problem is that of thrombogenicity as material-blood contact increases the risk of thrombus formation. Although any material could potentially be thrombogenic, some materials are less likely to initiate thrombus formation compared to others.

In considering which type of prosthesis is viable, a general overview of their pros and cons should be discussed. Advantages of mechanical valves include a longer mechanical lifetime lasting longer than the lifetime of the patient. However, patients undergoing mechanical prosthesis implantation must undergo lifetime anticoagulant

therapies such as coumadin (warfarin). This is due to the increased risk of thrombogenicity of mechanical valves. Biological valves have a shorter lifetime but do not require anticoagulant therapy. In addition, biological valves have smaller regurgitant volumes [5] often due to zero leakage volume [7].

[5]From [11], the Mosaic porcine has a regurgitant volume less than 1 mL/beat compared to the St. Jude Medical Regent aortic prosthesis' regurgitant volume of 13.5 mL/beat.

# Chapter 4

# The Fluid Mechanics of Heart Valves

The focus of this work is primarily from the perspective of functional hemodynamics rather than functional biomechanics. The latter considers the biosolid-fluid interaction to extensive detail and extracellular protein structure of the valve leaflet [12]. For the purposes of classification, cardiovascular fluid flow can be classified as a viscous, internal, and forced flow. Blood is generally considered a compressible fluid but can be assumed to be approximately incompressible for flow analysis in large arteries [13]. Since the SE and biological valve models created for the study do not possess orifice sizes comparable to the size of red blood cells, blood can be approximated as a Newtonian fluid[1]; thus the shear stresses can be calculated with knowledge of the velocity profiles. Although the general consensus is that blood is not a dilatant, the magnitude of blood's non-Newtonian nature is uncertain. Blood is a pseudoplastic (or shear thinning fluid) since the apparent viscosity decreases with the rate of deformation. Some work dealing with blood flow has modeled blood as a Bingham plastic or as a Hershel-Buckley fluid [14]. For the former case,

[1]Non-Newtonian means that the relationship between shear stress and the strain is nonlinear.

the shear stress is the product of the apparent viscosity and rate of deformation (as in the Newtonian case) plus a "residual" shear stress existing in the fluid in the absence of any deformation. The Hershel-Buckley approximation is similar to the Bingham plastic approximation with the exception of a higher residual shear stress and a subtle nonlinearity in the shear stress-rate of deformation relationship [15].

## 4.1 Valve Dynamics

Since the overall functioning of heart valves is similar for both sides of the heart, one can analyze the heart valve dynamics of either the left side or right side with little loss of generality. In this work, dynamics will be described in terms of the left side of the heart. The pressure and velocity profiles of the heart valves are shown in Fig. 4.1.

### 4.1.1 Atrioventricular Valve Dynamics

In the quiescent period, the heart is in a total relaxed state and oxygenated blood arrives from the pulmonary system and enters the left atrium. During this time, the AV valve (the mitral valve) hangs limply into the left ventricle as blood fills in from the left atrium. As the blood volume increases in the left ventricle, the blood pushes superiorly against the leaftlets and sets up the stage for atrial systole in order for the residual blood in the left atrium to be expelled into the left ventricle. This is followed by ventricular systole, in which the ventricle contracts and pushes blood superiorly against the leaflets to completely close the AV valve. At this point,

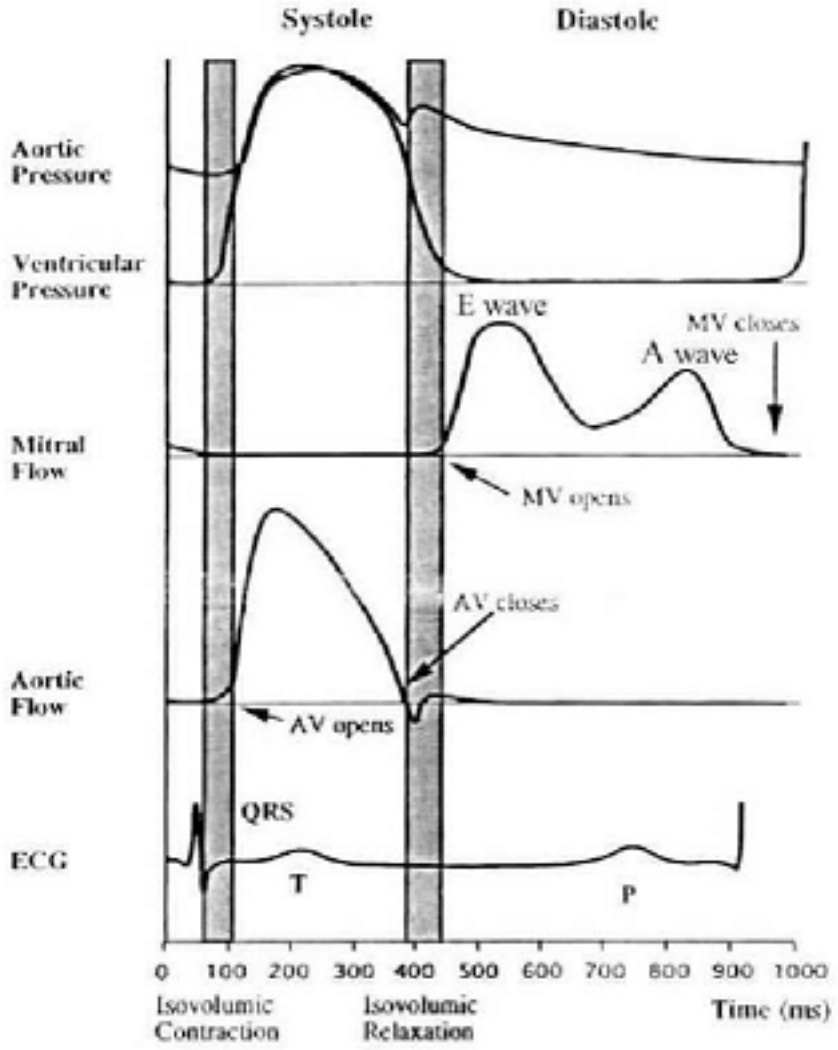


Figure 4.1: **Pressure-Velocity Profiles for Aortic and Mitral Valves (from [10])**: Peak pressure and velocity for the aortic occurs during ventricular systole. Aortic pressure peaks near mid-systole. During isovolumetric contraction, the aortic valve has an increase in pressure from the venticular side and increases to where it eventually overcomes the pressure on the aortic side and forces the aortic valve open. Velocity across the aortic valve peaks rather early during the ventricular systole phases but quickly deaccelerates (though not quite as fast as the initial acceleration phase).

the ventricle is a completely closed chamber and is the stage in the cardiac cycle referred to as the isovolumetric contraction stage.

Flow through the mitral valve has two distinct phases. In the quiescent period of the cardiac cycle, blood flows through the open mitral valve in what is termed the E-wave (first peak). The A-wave (the second peak) is due to atrial contraction. During the atrial systole, the residual blood in the atrium is forced into the ventricle. Healthy adults have a A-wave velocity that is slightly lower than the E-wave velocity (peak velocities during the E-wave are estimated to be from 0.5 to 0.8 m/s [7]). In reference to Fig. 4.1, the mitral flow has two localized peaks that correspond to the E-wave and the A-wave. The mitral valve opens for a longer duration of the cardiac cycle compared to the aortic valve, during which ventricular pressure decreases (due primarily to the ventricle being in diastole).

Pressure within the ventricle increases as the ventricle goes into systole. The additional pressure forces the mitral leaflets close.

### 4.1.2 Semilunar Valve Dynamics

During the isovolumetric contraction phase, ventricular systole continues and the rising ventricular pressure exceeds the aortic pressure, forcing the aortic valve open. The heart then goes into the quiescent period and with the ventricular pressure decreasing, blood flows back into the ventricle, effectively pushing superiorly against the SL leaflets and closing them. The aortic pressure is generally greater or comparable to the ventricular pressure due to the continual presence of blood (as opposed to the ventricle which starts receiving blood from the atrium as soon as

ventricular pressure becomes less than the atrial pressure).

Blood rapidly accelerates after the aortic valve opens, reaching its peak velocity in the first third of venticular systole. The blood flow starts to decelerate after reaching peak velocity, but not as quickly as the initial acceleration. Adverse pressure gradients cause the low inertial flow along the boundary to decelerate and then to reverse flow direction. The changes in flow direction result in vortices in the sinuses. The vortices are said to aid in the closure of the aortic valve but studies have shown that the pressure difference alone is sufficient to close the valve [12].

## 4.2 The Gorlin Equation

In natural heart valves, the blood flow is energy efficient as the valves involve little resistance to blood flow. In artificial valves and valves with stenosis, the valvular orifice produces greater resistance. Flow across an artificial valve experiences greater pressure drops across the valve.

The hemodynamic behavior of the aortic valve is related to the hemodynamics of the large arteries and so any detailed discussion of heart valve mechanics initiates at the ventricular outflow tract. The ventricular outflow is the rate of change of the ventricular volume and is pulsatile due to periodic ventricular contraction [13]. The stroke volume (SV) is defined as the amount of blood ejected out of the ventricle per beat. From a phenomenological perspective, stroke volume is the difference in ventricular volume at the end of diastole (EDV) and the ventricular volume at the

end of systole (ESV) so

$$SV = EDV - ESV \tag{4.1}$$

The dimensionless ejection fraction (EF) is the ratio of the volume that is ejected (SV) to the total resting volume (EDV):

$$EF = \frac{SV}{EDV} \tag{4.2}$$

The ejection fraction and cardiac output (CO) serve as clinical assessments of left ventricular performance. The cardiac output (for research and computational purposes) can be taken to be 5 L/min and is defined as the product of the stroke volume and heart rate (CO = SV x HR) [13]. As such, the stroke volume (volume per beat) can be written as the cardiac output divided by the heart rate. Dividing the stroke volume by the ejection time per beat ($t_E$) results in the volumetric flow rate per beat:

$$Q = \frac{CO}{HR \cdot t_E} \tag{4.3}$$

and from basic fluid mechanics, this is the product of the average flow velocity and the cross-sectional area per beat. Although this relationship is true, it remains rather ineffectual as it doesn't relate pertinent quantities such as pressure to readily measurable quantities such as the cardiac output or heart rate. One can ameliorate this situation by using the conservation of energy. The energy equation, like the Lagrangian and the Hamiltonian, is a conservative energy equation:

$$P_1 + \frac{1}{2}\rho_1 V_1^2 = P_2 + \frac{1}{2}\rho_2 V_2^2 \tag{4.4}$$

where P is the pressure, $\rho$ is the density, $V$ is the velocity, and we assume the potential energy difference is negligible. For an incompressible fluid, $\rho_1 = \rho_2 = \rho$ and so the energy equation becomes:

$$P_1 + \frac{1}{2}\rho V_1^2 = P_2 + \frac{1}{2}\rho V_2^2 \tag{4.5}$$

One assumes that point 1 is a geometric location with a very small velocity compared to the jet velocity of point 2. It is relevant to note that while blood is generally compressible, this doesn't play a factor in the analysis as the small velocity approximation removes any effect of the density at point 1. Solving for the velocity at point 2 leads to:

$$V_2 = \sqrt{\frac{2\Delta P}{\rho}} \tag{4.6}$$

where $\Delta P = P_1 - P_2$. Since the volumetric flow rate is the product of the average flow velocity and the cross-sectional area, this implies:

$$\frac{CO}{HR \cdot t_E} = A\sqrt{\frac{2\Delta P}{\rho}} \tag{4.7}$$

While this relates valve cross-sectional area, volumetric flow rate, and pressure drop, it is unrealistic because the energy equation doesn't allow for dissipative factors. Realistically, heart valves impose significant viscous losses. According to [4], two nonideal conditions are associated with flow across the valve. The first is the previ-

ously mentioned viscous forces and the second is the jet flow contraction (where the jet of blood across the valve is smaller than the total cross-sectional area). The first nonideal case is circumvented by dividing the velocity by a valve constant $C_V$. The valve constant incorporates the frictional losses incurred from flow through the valve [16]. For the second nonideal case, the area of contraction $A$ is proportional to the cross-sectional area $A_V$ and the constant of proportionality is the valve coefficient $C_C$. As such, the volumetric flow rate can be written

$$Q = \frac{CO}{HR \cdot t_E} = C_V \sqrt{\frac{2\Delta P}{\rho}} C_C A_V \tag{4.8}$$

Solving for the cross-sectional area:

$$A_V = \frac{1}{C_V C_C} \sqrt{\frac{\rho}{2}} \frac{CO}{HR \cdot t_E} \frac{1}{\sqrt{\Delta P}} \tag{4.9}$$

This is the Gorlin equation and it serves as a clinical assessment of flow impedance across a heart valve. The Gorlin equation outputs an effective orifice area (EOA) which allows for physicians and engineers to properly analyze proper flow dynamics across the heart valve.

The valve coefficients, density, and the square root of 2 are often lumped together (for clinical purposes) as a valve-dependent coefficient $K$ (called the Gorlin constant). The Gorlin constant is defined as:

$$K = C_V C_C \sqrt{\frac{2}{\rho}} \tag{4.10}$$

and has units of $\frac{[L]}{[T] \cdot [P]^{1/2}}$ and for clinical purposes, the units are often taken to be:

$$K \rightarrow \frac{cm}{s\sqrt{mmHg}} \tag{4.11}$$

With this, the Gorlin equation becomes:

$$A_V = \frac{CO}{HR \cdot K \cdot t_E} \frac{1}{\sqrt{\Delta P}} \tag{4.12}$$

The Gorlin constant is not technically a constant since the valve coefficients may fluctuate under varying Reynolds numbers but for standard conditions, $K$ can be assumed constant. According to [4], $K$ is taken to be approximately 44.3 for aortic valves and 37.7 for mitral valves.

In order to make the Gorlin equation consistent unit-wise, the cardiac output should be given in mL/min, the heart rate in beats/min, and the ejection time in seconds. The effective orifice area will be given in units of $cm^2$. The Gorlin equation remains a useful tool in analyzing the flow dynamics across heart valves. It provides a quantitative assessment in regards to flow impedance.

# Chapter 5

# Modeling Considerations and Methodology

CFD modeling and analysis of the heart valves utilized commercial software CFD-GEOM, CFD-ACE, and CFD-VIEW for all steps of the analysis. The CFD-GEOM software was used to create the geometric model of the heart valve, designate boundaries for the model, and for grid generation. CFD-ACE was used for the solution phase while CFD-VIEW was used for the post-processing phase. Although a transient model would be desirable considering the unsteady flow physics of the heart valve, valve (be it leaflet or ball occluder) position-flow dynamics coupling remains a significant challenge. In order to circumvent this difficulty, models at different parts of the cardiac cycle were created to capture the dynamics at certain times (early ventricular systole and at mid-to-late ventricular systole when peak velocity is reached). Each model was configured to calculate pressure, velocity, turbulent kinetic energy, and hemolysis percentage.

## 5.1 Pre-Processing

The pre-processing stage involved creating the geometry and meshing. Due to the difficulty of modeling a complex (and dynamical) structure such as the sino-tubular junction and aorta, the model was simplified to a steady-state geometry and several fluid parameters (such as the density and inlet parameters) were assumed to be constant. The primary benefit of using a constant geometry model is that one avoids having to remesh the computational domain after every iteration. The difficulty of this is exacerbated if one wishes to incorporate a detailed fluid-structure coupling (in which case both computational domains have to be remeshed for every iteration). Although this seems to be unrealistic, this approach was appropriate since the computational domain was modeled at an instant in the cardiac cycle (one assumes that the time duration is small enough so that the changes in the overall geometry are negligible).

## 5.2 Turbulence Models

Turbulent flow in the cardiovascular system is characterized by random motion in blood cell trajectories. The difficulty associated with modeling turbulent flow is due to the stochastic nature of the dynamics, making a deterministic assessment virtually impossible. The fluctuations in the blood cell motion give rise to eddies that enhance momentum and energy transfer. The turbulent shear stress that result from the enhanced momentum and energy transfer is a sum of a laminar component and a turbulent component [17]. The laminar component accounts for frictional effects between layers in the direction of flow while the turbulent component accounts

for the frictional effects between the blood cells. Several fluid dynamical models to analyze turbulence have been proposed. Some of the earlier models (like the Boussinesq and Prandtl models) for turbulence are simple compared to the current models. The Boussinesq model suggests that the turbulent shear stress is proportional to the spatial gradient of the average velocity:

$$\tau_{turbulent} = \mu_t \frac{\partial \bar{u}}{\partial y} \tag{5.1}$$

where $\mu_t$ is the eddy viscosity [17]. The eddy viscosity accounts for the momentum transport involved with the turbulent eddies. The Prandtl model states that the turbulent shear stress component is proportional to the *square* of the spatial gradient of the average velocity component:

$$\tau_{turbulent} = \rho l_m^2 \left( \frac{\partial \bar{u}}{\partial y} \right)^2 \tag{5.2}$$

where $l_m$ is the mixing length (the distance a particle travels before colliding with other particles[1]) [17]. The mixing length is often difficult to determine and is not constant for a given flow. Hence the Prandtl model is not used as extensively as the current k-$\epsilon$ models of turbulence. The k-$\epsilon$ models utilize the concept of eddy viscosities on the macroscale to analyze turbulence rather than focus on local fluctuations. The k-$\epsilon$ or k-$\omega$ models[2] often employed have their foundations within the RANS (Reynolds Averaged Navier-Stokes) theoretical framework. The RANS framework utilizes an averaging operation to account for the fluctuations and decompose the stochastic flow fields into average values [18].

[1]This is conceptually similar to the mean free path in the kinetic theory of gases.

[2]Turbulence models for CFD simulations involve two extra transport equations: one for the kinetic energy (k) and the other for either the dissipation $\epsilon$ or specific rate of dissipation $\omega$.

Choice of a k-$\epsilon$ turbulence scheme is dependent on the objectives of the simulation. For blood flow, high Reynolds methods such as the Launder-Spalding version of the k-$\epsilon$ theory or the RNG (Renormalization Group) k-$\epsilon$ model can be used. For this work, the former model is used.

### 5.2.1 The Launder-Spalding k-$\epsilon$ Model

The Launder-Spalding model is a k-$\epsilon$ method for mean flow behavior dynamics with an emphasis on computational economy, range of applicability, and physical realism [19]. For the Launder-Spalding model, the turbulent viscosity $\nu_t$ is defined as

$$\nu_t = \frac{C_\mu k^2}{\epsilon} \tag{5.3}$$

where $C_\mu$ is a Launder-Spalding constant (one of five used for this particular model), $k$ is the turbulent kinetic energy term, and $\epsilon$ is the turbulent dissipation rate. The transport equations used for the turbulent kinetic energy and turbulent dissipation rate are:

$$\frac{\partial}{\partial t}(\rho k) + \frac{\partial}{\partial x_j}(\rho u_j k) = \rho P_{prod} - \rho\epsilon + \frac{\partial}{\partial x_j}\left[\left(\mu + \frac{\mu_t}{\sigma_k}\right)\frac{\partial k}{\partial x_j}\right] \tag{5.4}$$

$$\frac{\partial}{\partial t}(\rho \epsilon) + \frac{\partial}{\partial x_j}(\rho u_j \epsilon) = C_{\epsilon_1}\frac{\rho P_{prod}\epsilon}{k} - C_{\epsilon_2}\frac{\rho\epsilon^2}{k} + \frac{\partial}{\partial x_j}\left[\left(\mu + \frac{\mu_t}{\sigma_\epsilon}\right)\frac{\partial \epsilon}{\partial x_j}\right] \tag{5.5}$$

where the $P_{prod}$ is the production term defined by [18] as

$$P_{prod} = \nu_t \left( \frac{\partial u_i}{\partial x_j} + \frac{\partial u_j}{\partial x_i} - \frac{2}{3} \frac{\partial u_m}{\partial x_m} \delta_{ij} \right) \frac{\partial u_i}{\partial x_j} - \frac{2}{3} k \frac{\partial u_m}{\partial x_m} \tag{5.6}$$

In the preceding equations, $u$ denotes a velocity component, $x$ is a coordinate, and $\delta_{ij}$ is the Kronecker delta (which is 1 if $i = j$ and 0 if $i \neq j$). The set of parameters $\{C_\mu, C_{\epsilon_1}, C_{\epsilon_2}, \sigma_k, \sigma_\epsilon\}$ represents the constants used in this k-$\epsilon$ model. The values for these constants are set by [18] to be: $C_\mu = 0.09$, $C_{\epsilon_1} = 1.44$, $C_{\epsilon_2} = 1.92$, $\sigma_k = 1.0$, and $\sigma_\epsilon = 1.3$. These values are the default values used in CFD-ACE simulations.

## 5.3 Geometrical Considerations

The choice for a computational domain for the aortic valve can vary depending on the information required. For hemodynamic analysis on the local scale (such as structural-fluid interaction, coronary inlet conditions, etc.), the computational domain can contain the region inferior to the sinotubular junction (in the left ventricle) and can extend to just include the sinus of Valsalva. For detailed calculation of downstream turbulence effects, a computational domain that extends to the arch of the aorta would be appropriate.

The computational domain used for simulations in this work includes the upper left ventricle, sinotubular junction, sinus of Valsalva, and extension into the aorta. This is shown in Fig. 5.1.

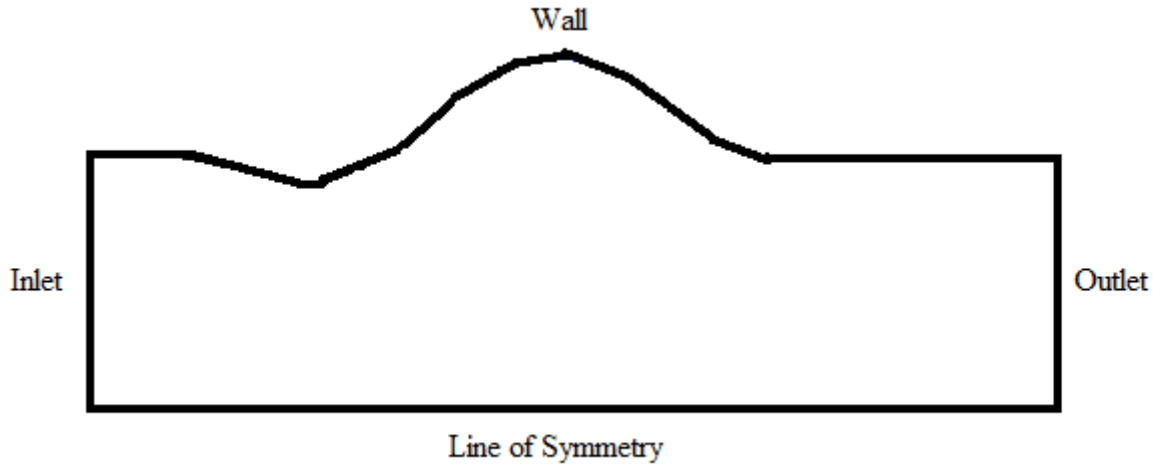


Figure 5.1: **General Graphical Depiction of the Computational Domain:** The computational domain shown does not include the valve structure.

Simplified models of the sinutubular junction and adjacent aorta suggest an axisymmetrical configuration that is utilized for 2D modeling. Realistically, the sinuses of Valsalva remove any suggestion of symmetry. Even using a sectioned modeling (cylindrical modeling that considers a third of the aortic cross-section) is at a disadvantage as two of the sinuses give rise to the coronary arteries and the third sinus (the right posterior sinus) is non-coronary. However, sectioned modeling can provide a reasonable analysis for bioprosthetic valves at mid-systole since the leaflets in their open configuration divert flow past the sinuses of Valsalva. Three-dimensional modeling, while more complicated and demanding of computational resources, eliminates two-dimensional models' inability to model the intrinsic asymmetries of the aortic outflow tract. Despite the drawbacks, 2D modeling remains desirable due to simplicity and fewer computational resources required in grid generation.

Although material considerations are not considered in this work, a suitable fluid-structure coupling scheme remains an objective in heart valve simulations. Modeling the human heart valve leaflet poses a considerable task since the leaflet is anisotropic due to the composite layering of fibrosa, spongiosa, and ventricularis. What exacerbates the difficulty of modeling the human leaflet is that the primary layer (the spongiosa) does not transmit stress in proportion to its thickness. Fortunately, for bovine pericardial tissue-based heart valves, the leaflets are approximately isotropic and the functional thickness (which can be an uncertain parameter in natural heart valve leaflets) can be assumed to be the thickness of the pericardial leaflet [5]. For silicone-based ball valves, the material can be assumed to be isotropic.

Focus of the hemodynamic performance centered on two types of valves: the aortic SE valve and an aortic bioprosthetic valve[3]. Creating the geometric model relied on four assumptions:

1. Although blood flow through the aortic valve is pulsatile, the heart valve is modeled as a steady-state system at certain time steps. Each state has a specified inlet pressure and inlet velocity determined by analyzing pressure/velocity plots found in [10]. This is necessary due to intrinsic difficulties in modeling transient flow.

2. The aortic diameter remains essentially constant. In reality, aortic dilation has been reported in sheep [20] but for modeling purposes, the aortic diameter

[3]The bioprosthetic valves are biological leaflet valves derived from gluteradehyde-treated porcine aortic valve leaflet or bovine pericardial tissue.

can be assumed approximately constant since modeling takes place at discrete time frames.

3. The computational domain is a thin slice in the $z$ direction rather than axisymmetrical. The reason for this configuration is due to the intrinsic asymmetry of the aorta because of the sinuses of Valsalva and the presence of the coronary ostia. Axisymmetry is not assumed due to the length disparities along the radial axis of the leaflet and the apposition zones of the valve. Using an axisymmetric model results in CFD-ACE interpreting the heart valve to be a conical Venturi tube (which leads to extremely high jet velocities at peak systole).

4. The location of the SE valve at peak velocity is assumed to be central. In reality, the position of the SE valve at times following the early ventricular systole is eccentric with respect to the axis of symmetry but one can take the average position to be central. For the biological valve, the leaflet's free margin oscillates at peak velocity, but, as in the case of the SE valve, the average position is modeled.

The geometric model is set up in a two-dimensional configuration by creating three distinct entities: the ventricle, the aortic root[4], and the aorta. In order to create a reasonably realistic model, a comparative study of surgical and anatomy references is required.

[4]This includes the sinotubular junction and the sinus of Valsalva

### 5.3.1 Meshing

The geometries of the valves and an appropriate grid patterns are created using CFD-GEOM. CFD-GEOM offers three types of meshes: unstructured triangular meshing, hybrid meshing (with quad meshing being dominant), and quadrilateral meshing. Irregular arcs in the system prevent a structured grid from being an appropriate choice. A triangular meshing scheme is used for both the SE and the biological valve. These meshes are shown in Fig. 5.2 and Fig. 5.3. The mesh transition factor of 1.1 is the default value for both models. The mesh transition factor is the parameter that sets an upper bound on the ratio of lengths of grid segments composing the mesh. This selected value of 1.1 for the mesh transition factor is appropriate since a mesh transition factor less than 1.01 may lead to divergent solutions and larger mesh transition values may lead to a coarser grid. This ensures the ratio of one grid segment's length to a smaller, adjacent grid segment's length will not exceed the mesh transition factor [21]. The mesh transition factor controls the global mesh growth rate during the triangular surface grid generation.

## 5.4 Methodology

### 5.4.1 Pressure

The pressure and velocity distributions of the aortic valve have been measured by analyzing pressure and velocity profiles to determine corresponding values at early systole and peak velocity. A mean peak velocity of 1.35 m/s was used in simulations as the inlet velocity. To model hemodynamics in children, the mean

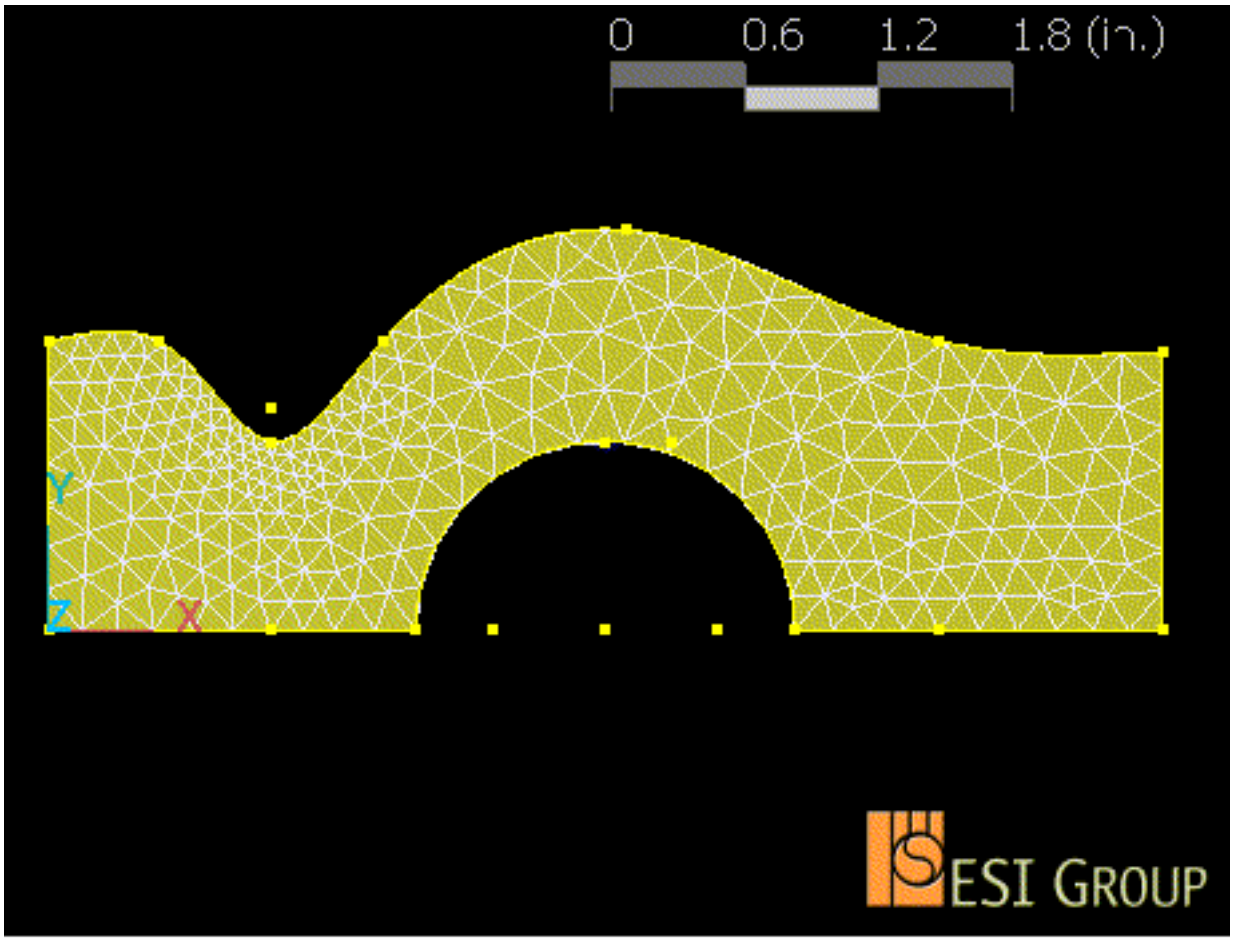


Figure 5.2: **Meshing Scheme for the SE Valve at Peak Velocity:** The mesh pattern is an unstructured triangular meshing with a mesh transition factor of 1.1 (the default for CFD-GEOM). Since the model is a steady-state model and the simulation does not consider fluid-structure coupling, the geometry does not need to be remeshed for each iteration.

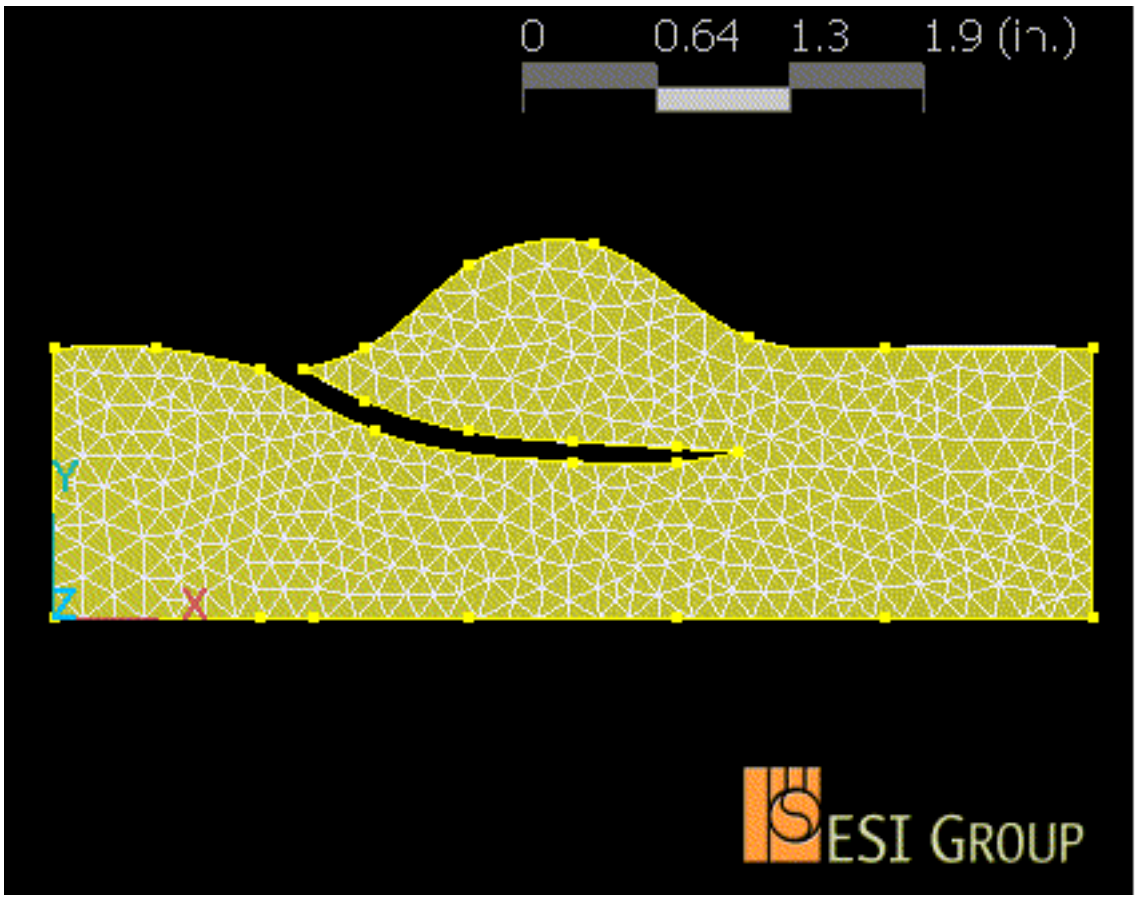


Figure 5.3: **Meshing Scheme for the Biological Valve at Peak Velocity:** The mesh pattern is an unstructured triangular meshing with a mesh transition factor of 1.1 (the default for CFD-GEOM).

peak velocity will be higher (1.5 m/s) [7]. A velocity and pressure at early systole can be approximated graphically using Fig. 4.1. The plot is scaled assuming a maximum aortic pressure of 120 mmHg and a minimum pressure of 80 mmHg. Using this scaling, pressure at early systole was taken to be approximately 107 mmHg and approximately 115 mmHg at peak velocity. The aortic velocity at early systole is approximated to be 1.27 m/s. These values were used as velocity boundary conditions at the inlet.

Pressure is a significant parameter to measure in artificial heart valves since ideal heart valves should effectively minimize pressure drops across the valve. The pressure drops in this work were calculated by comparing[5] average pressure downstream (typically starting near the posterior structure of the heart valve) to the inlet pressure.

The boundary conditions specified for each model were obtained from [7] and [10]. This work used the aortic peak velocity of 1.35 m/s for the inlet velocity.

### 5.4.2 Shear Stresses

A subroutine was written specifically for calculating shear stresses along a designated surface. The surface name had to be specified within the body of subroutine. The subroutine was required since CFD-ACE did not have a built-in feature for calculating shear stresses. With the Newtonian approximation, shear stresses take

[5]The pressure is calculated by averaging pressure values along a line perpendicular to the flow axis.

the form

$$\tau = \mu \frac{\partial u}{\partial y} \tag{5.7}$$

where $\mu$ is the dynamic viscosity, $y$ is the distance from the surface, and $u$ is the component of the velocity that is orthogonal to the plane of the surface.

### 5.4.3 Hemolysis

Hemolysis is the destruction of red blood cells which results in releasing hemoglobin into the ambient plasma. Intervascular hemolysis as it pertains to heart valves can result from flow across *in vivo* devices with sagittal projections or rough surfaces. The model of choice for hemolysis simulations is a modified version of the Giersiepen model:

$$\frac{\Delta Hb}{Hb} = A\tau^B t^C \tag{5.8}$$

where $\tau$ is the shear stress in Pa, $t$ is the residence time, and $A$, $B$, and $C$ are pre-defined constants [18]. The term $\frac{\Delta Hb}{Hb}$ is the percentage of hemoglobin released by the red blood cells within the vacinity of the valve structure. CFD-ACE-based computational simulations using the Giersiepen model have default values of $A = 3.62 \times 10^{-5}$, $B = 2.416$, and $C = 0.785$. The residence time is the time duration in which red blood cells are exposed to the valve prosthesis and the damage mechanism of hemolysis is directly affected by the residence time of the cell in the environment.

# Chapter 6

# Post-Processing and Discussion

## 6.1 Post-Processing

The solution phase was conducted using CFD-ACE and post-processing utilized CFD-VIEW. The CFD simulations utilized the Navier-Stokes equations which CFD-ACE solves by iterative methods (the Navier-Stokes equations are briefly discussed in Appendix A). Pertinent quantities such as pressure drop, velocity profile, turbulent kinetic energy, shear stresses, and hemolysis were analyzed for each model at peak velocity and compared to determine the relative improvements of the biological valve compared to the SE valve.

### 6.1.1 Pressure Drop

The pressure drop across both models was evaluated by selecting an average value of the pressure near the inlet and subtracting an average value of the pressure at a point significantly far from the valve structure. The pressure values along a line of constant $x$ (referring to Fig. 5.2 and Fig. 5.3) were evaluated and averaged

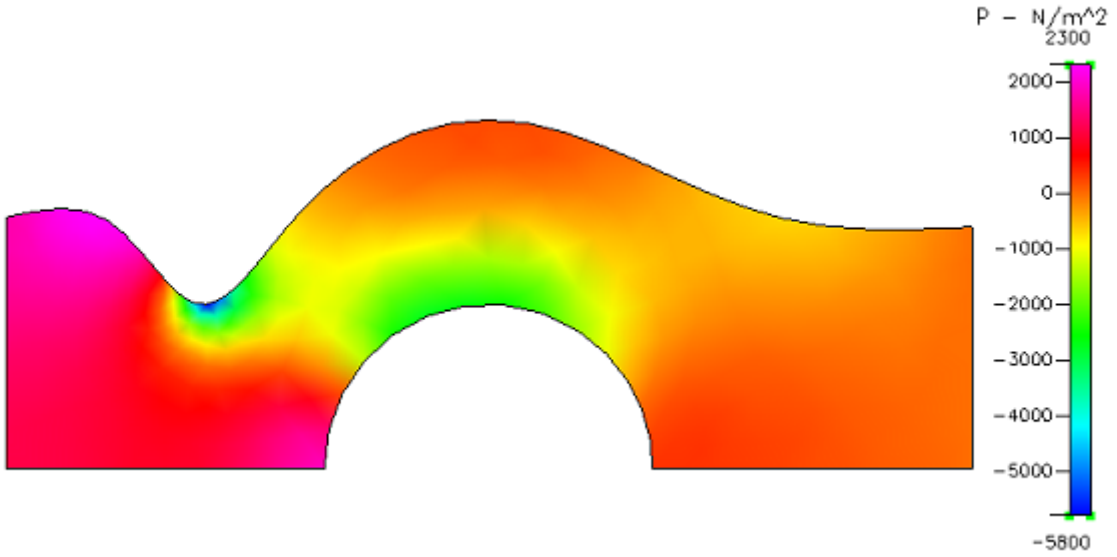


Figure 6.1: **Pressure Plot of SE Valve at Peak Velocity:** Pressure changes are most drastic in the vicinity of the orifice structure. This poses a concern for engineering designs as localized pressure gradients are tied into cavitation damage of the overall valve structure.

to obtain the value used in the pressure drop calculation. The average pressure for the SE valve (the pressure near the inlet) was calculated to be 1546.13 Pa and the average pressure for the biological valve was calculated to be 714.62 Pa.

The localized pressure drop in Fig. 6.1 in the orifice region is cause for concern since localized pressure reductions (to pressure values below the liquid vapor pressure) lead to rapid formation and collapse of bubbles (cavitation). The bubbles (called nuclei) collapse if the ambient pressure exceeds the pressure within the nuclei. Because of the rapid nature of the bubble formation/collapse, generated shock waves [7] could cause damage to the nearby structures. For the pressure plot in the biological valve (Fig. 6.2), a lower pressure corresponds to the high-velocity jet flowing near the leaflet surface (Fig. 6.4). The calculated average pressure drop

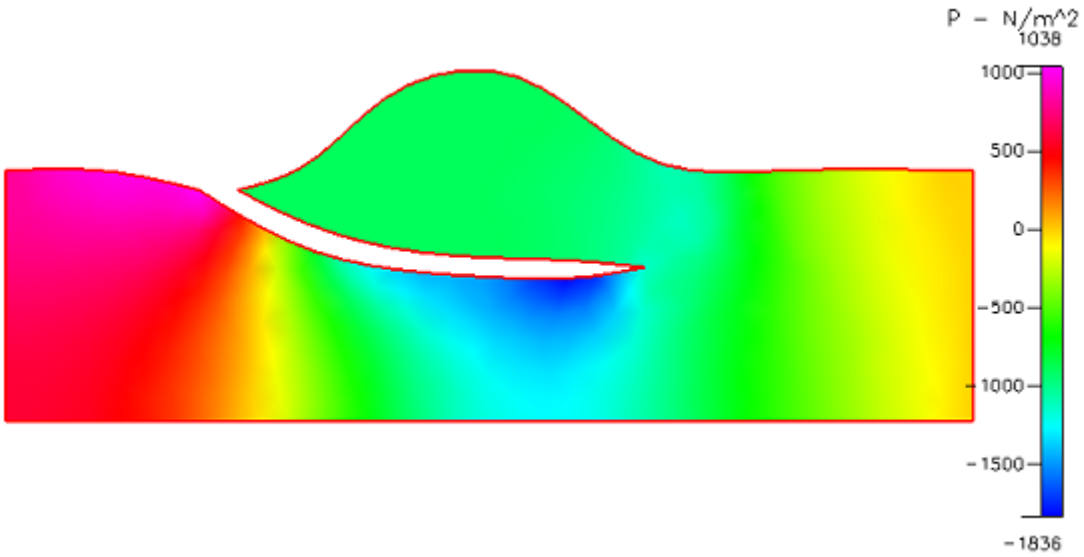


Figure 6.2: **Pressure Plot of Biological Valve at Peak Velocity:** The reduction in pressure near the leaflet is due to the "jetting" confirmed by [7]. Although not verified, it can be speculated that this reduction in pressure aids in the closure dynamics of the valve. Based on this plot, if the valve remained open for a longer time duration (the normal time scale on the order of $10^{-6}$ s), there would be a significant amount of stress in the leaflet's basal attachment.

across the biological valve of $\Delta P_{Bio} = 870.2$ Pa $\approx 6.5$ mmHg. This is roughly 54% the pressure drop of the SE valve (measured at the same locations for the previous calculation). Calculation of the pressure drop across the SE valve leads to a figure of $\Delta P_{SE} = 1600.7$ Pa $\approx 12.0$ mmHg. Since pressure drops are to be minimized, results indicate that the biological valve performs better compared to the SE valve in terms of pressure drops.

### 6.1.2 Velocity

Velocity and flow patterns are of vital interest since significant velocity changes are associated with turbulence. In addition, locations of flow stagnation could be a

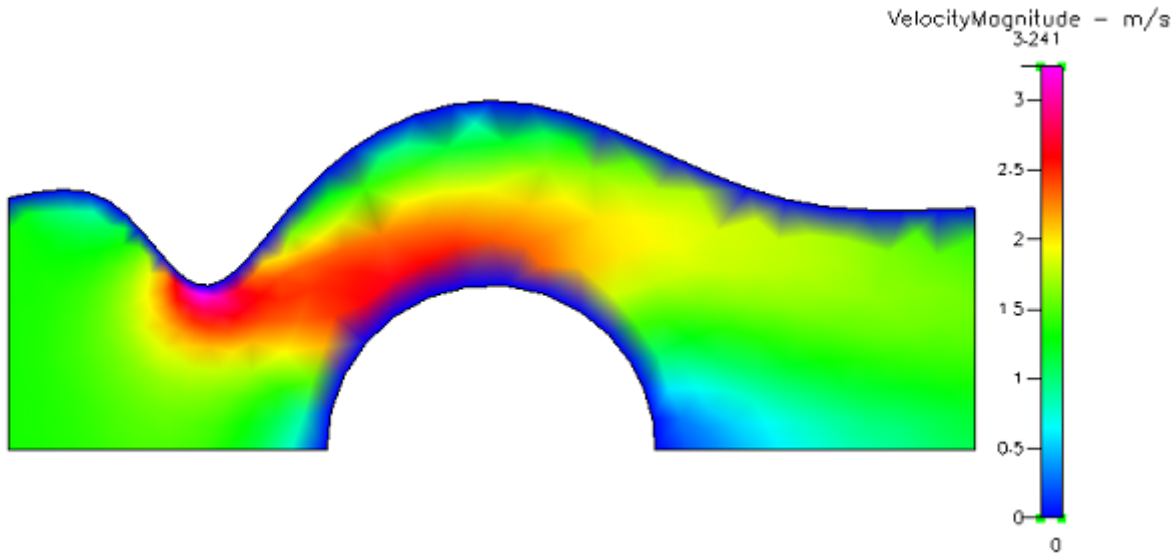


Figure 6.3: **Velocity Plot of SE Valve at Peak Velocity:** The orifice boundary (which was designed to be hemodynamically efficient) caused an increase in velocity in the blood flow but decelerated within the vicinity of the valvular structure.

potential source of thrombus formation. Velocity plots of both valves are shown in Fig. 6.3 and Fig. 6.4. For both simulations, the velocity at the inlet is taken to be the average aortic peak velocity of a healthy adult (1.35 m/s).

For the SE valve Fig. 6.3 shows the sudden acceleration of blood near the ventricle side of the orifice. It is speculated this acceleration is due to a localized pressure drop in the vicinity of the orifice. Referencing Fig. 6.3, one can see the velocity gradient from the ball occluder surface to the neighboring flow field. This is due to the enforced "no-slip" condition at the valve surface. The resulting turbulence due to this gradient is unavoidable and occurs regardless of the valve prosthesis.

The biological valve in Fig. 6.4 shows a significant jetting across the valve adjacent to the ventricularis. Computational simulations as reported in [7] have shown

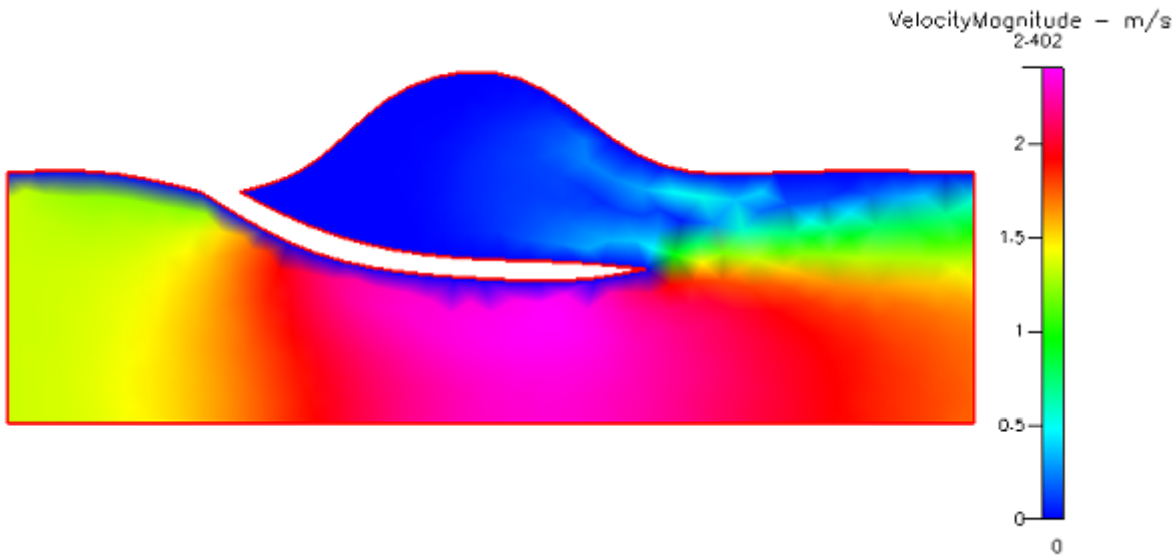


Figure 6.4: **Velocity Plot of Biological Valve at Peak Velocity:** The velocity experiences an increase in the valvular region adjacent to the leaflet surface. The velocity is not uniform in the region posterior to the leaflet tip. The small velocities in the sinus region coming in contact with the higher velocities across the valve leaflet can lead to turbulence.

that this jet velocity can be significantly high. Had the model utilized axisymmetry, the geometry of the biological valve would have been interpreted as a conical shape, increasing the velocity near the marginal ends of the leaflet. A simulation at early systole using axisymmetry was performed and the jet velocities near the marginal ends of the leaflet were determined to be on the order of 20 m/s. A calculation using the continuity equation can confirm this high velocity. The velocity at early systole as taken from [10] to around 1.3 m/s (which is determined from the scaling the velocity profile). If the leaflet "tip" is located approximately 0.3 cm from the line of symmetry and the orifice radius of 1.2 cm, then the continuity equation for an incompressible fluid gives a velocity of:

$$v = \frac{1.35\frac{m}{s}\left(1.2cm\right)^2}{\left(0.3cm\right)^2} \approx 22\frac{m}{s} \tag{6.1}$$

With any valve (native or prosthetic), the deviance from a perfect cylindrical configuration will cause inevitable changes in velocity within the vicinity of the valve structure and so velocity profiles posterior to the valve structure should be analyzed to determine a valve's long-term effect on velocity and turbulence. Two velocity profiles (taken approximately 3 cm from the sinotubular junction) are shown in Fig. 6.5 and Fig. 6.6. A fully developed laminar velocity profile has an approximately parabolic shape due to adherence to the "no slip" condition at the surface-fluid interface and the retardation of fluid motion in adjacent layers due to shear stresses. The velocity profile of the SE valve (in Fig. 6.5) shows a very large increase in velocity near the aorta wall. From Newton's viscosity law, this implies a large shear stress associated with the flow in the vicinity.

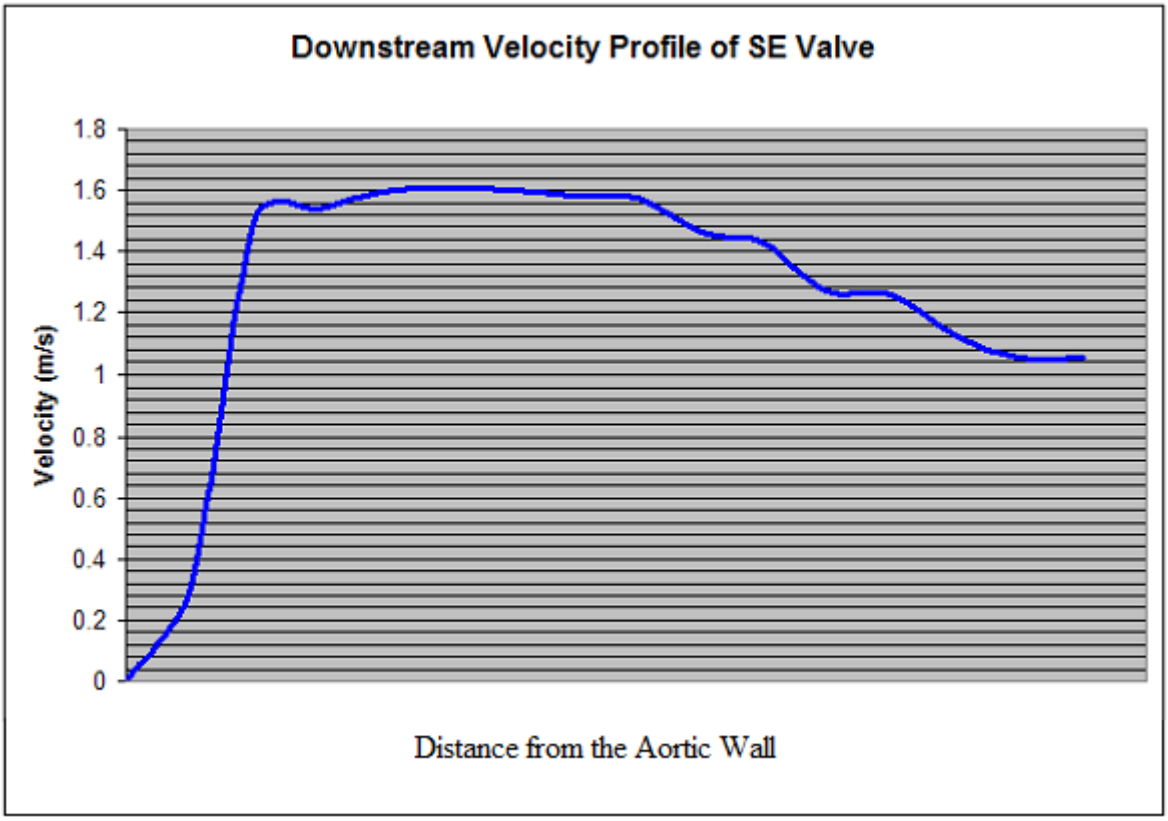


Figure 6.5: **Velocity Profile of the SE Valve:** Velocity profile was calculated at approximately 3 cm from the sinotubular junction. The $x$-axis is the distance from the aortic wall. The flatter velocity profile (in comparison to a parabolic laminar flow profile) indicates turbulent flow. The plot shows the viscous sublayer and the subtle transition into the buffer sublayer. The turbulent layer is marked by where the velocity profile becomes flatter.

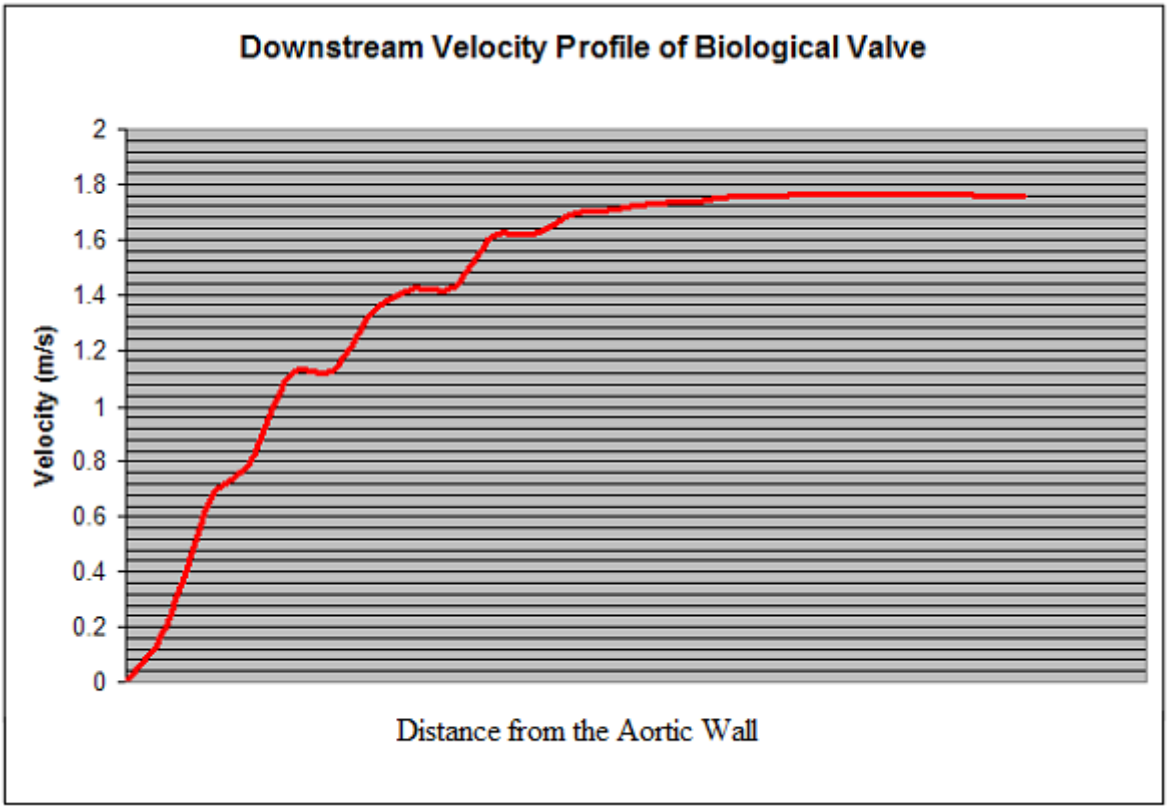


Figure 6.6: **Velocity Profile of the Biological Valve:** Velocity profile was calculated at approximately 3 cm from the sinotubular junction. The $x$-axis is the distance from the aortic wall. Velocity profile indicates an approximately fully developed flow with some indications of turbulent flow (indicated by the "zigzag" form near the vessel wall).

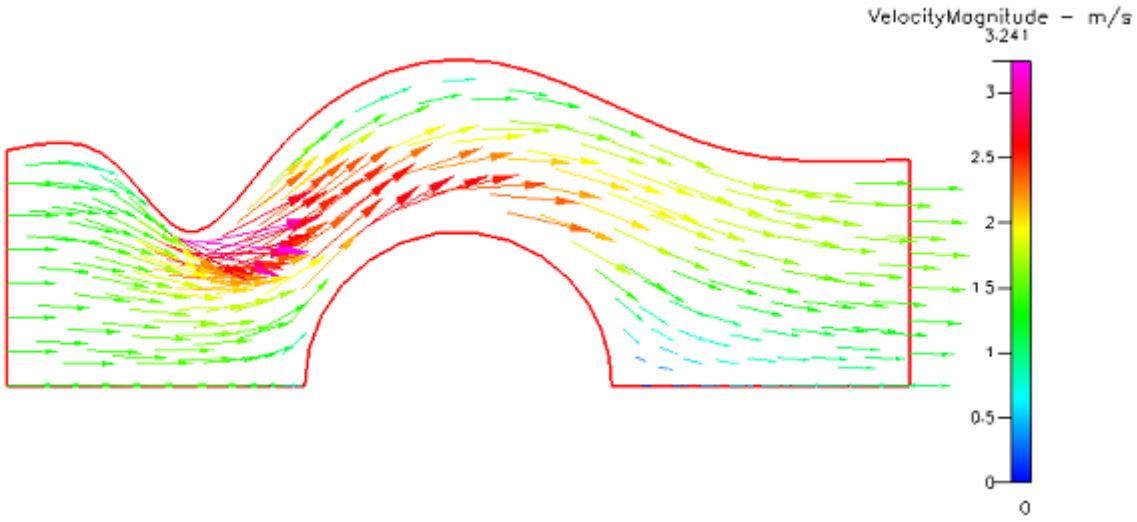


Figure 6.7: **Flow Pattern of the SE Valve At Peak Velocity:** The density of flowlines increases in the location of the orifice and decreases upon entry into the sinus of Valsalva. Although not shown in detail in this plot, the posterior location of the ball occluder along the line of symmetry (right side of the ball) is a location of flow separation during venticular systole.

### 6.1.3 Turbulent Kinetic Energy

Large turbulent kinetic energy is to be avoided in a heart valve prosthesis. This is because the kinetic energy is proportional to the linear momentum:

$$T = \frac{p^2}{2m} \tag{6.2}$$

where $T$ is the kinetic energy, $p$ is the momentum, and $m$ is the mass. The presence of large kinetic energy associated with flow corresponds to large momentum involved. Fig. 6.9 shows the turbulent kinetic energy and its relationship to the distance posterior to the valve (and extending to the outlet). The turbulent kinetic energy of the biological valve decreases considerably in the direction of flow in comparison

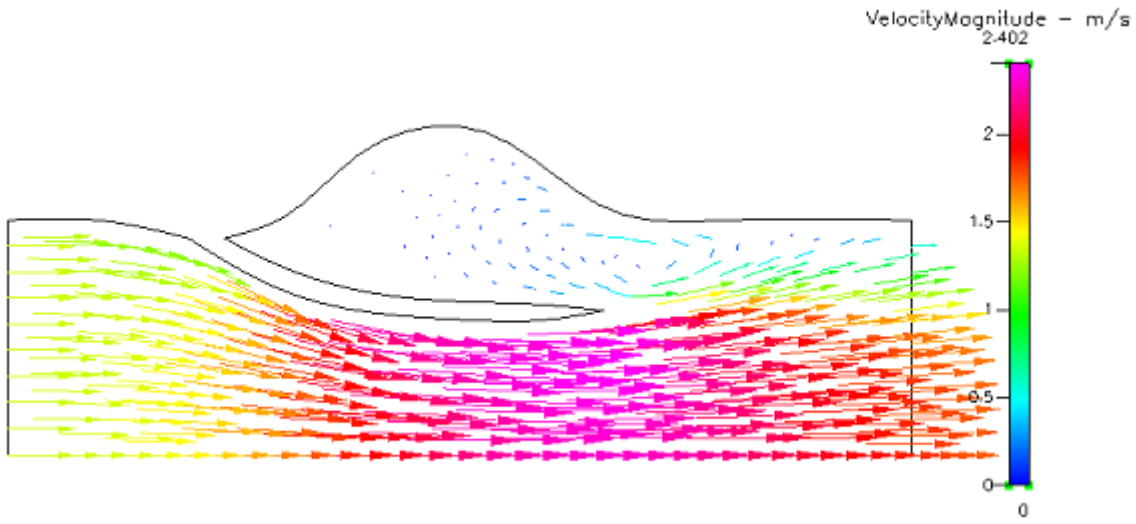


Figure 6.8: **Flow Pattern of the Biological Valve At Peak Velocity:** There is a high density of flow lines beneath the leaflet surface due to the decrease in the effective cross sectional area. During ventricular systole, the sinus of Valsalva experiences some recirculation. The marginal end of the leaflet creates a location of flow separation that is adjacent to two fluid layers at different velocities. The figure shows that vicinity of the leaflet attachment on the fibrosa side (next to the sinus) experiences very little blood flow during peak velocity. The retrograde blood flow during the deacceleration phase and subsequent closure of the valves allow for proper blood circulation into the sinus.

to the SE valve. The biological valve has a slightly higher turbulent kinetic energy near the leaflet free edge and this initially high turbulent kinetic energy value is speculated to be due to the intrinsic nature of the leaflet morphology since the leaflet free edge will change the velocity of the local blood flow considerably. Since turbulence production should be minimized, this analysis of the turbulent kinetic energy indicates that the biological valve possesses hemodynamic improvement over the SE valve.

### 6.1.4 Shear Stresses

A subroutine was used to calculate shear stresses along boundaries that were specified within the code of the subroutine. The total shear stress in the SE simulation was 42.3 $N/m^2$ while the total shear stress in the biological valve was calculated to be 36.0 $N/m^2$. One can speculate that the reduction in shear stresses is due to the minimized turbulence effects of the biological valve but both calculated values are below the shear stress threshold for hemolysis ($\approx$ 400 to 600 $N/m^2$) [7]. The threshold values are figures used in computational stress analysis of heart valve fluid dynamics.

### 6.1.5 Hemolysis

The hemolysis measurement produced higher hemolysis percentages for the SE valve compared to the biological valve (1.14% for the biological valve compared to 1.29% for the SE valve). Although both of the models had an output of significantly low hemolysis percentages, the biological valve should have an even lower percentage then calculated. This can be explained by limitations of the two-dimensional

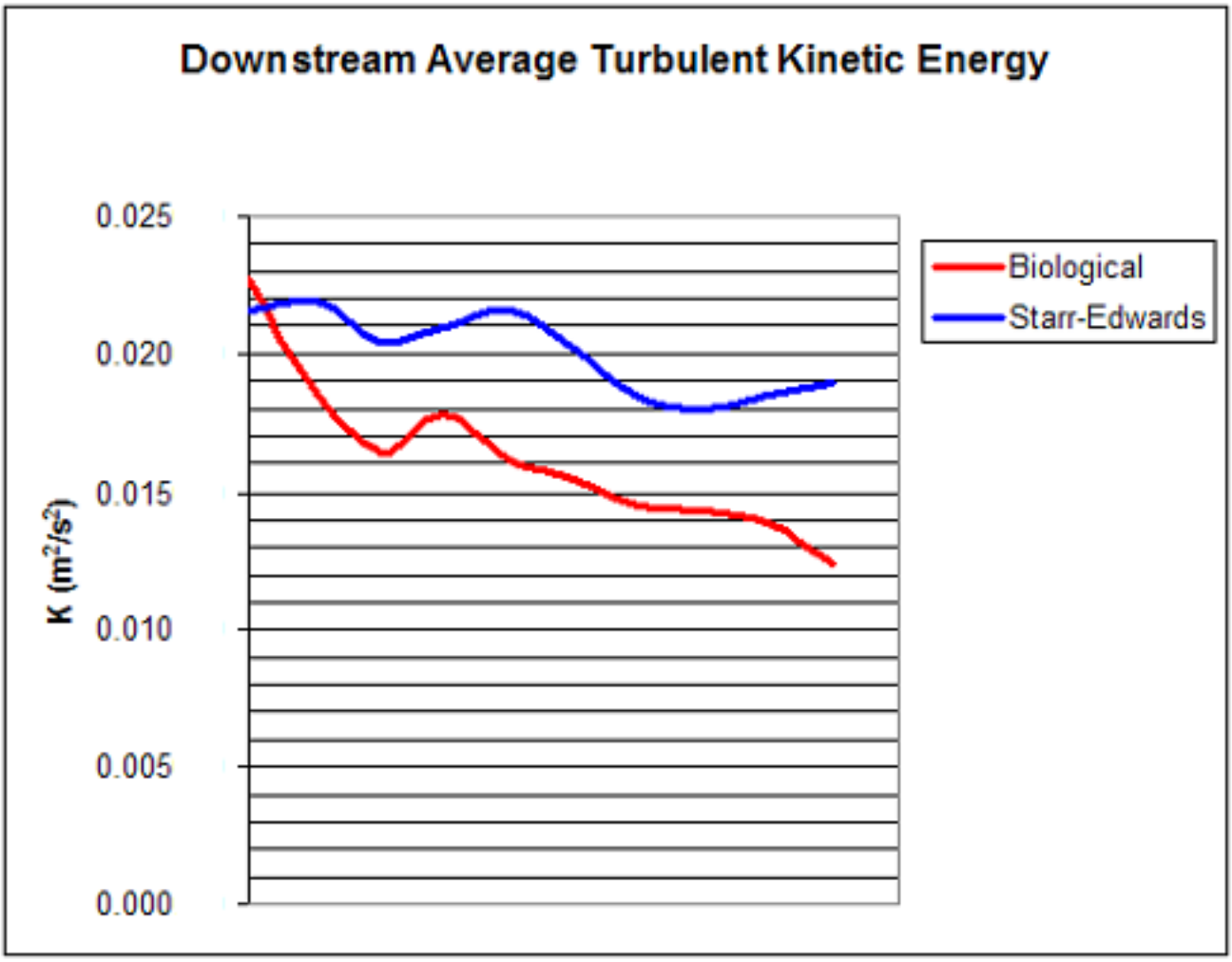


Figure 6.9: **Turbulent Kinetic Energy:** The plot shows the turbulent kinetic energy as a function of distance posterior to the valve. Turbulent kinetic energy values are measured starting at approximately 4.5 cm from the inlet. The initial higher value in the biological valve is due to the leaftlet creating a drastic velocity change tied into turbulent physics.

geometric model as the CFD software interprets the leaftlet margin as an apical edge, thus increasing the percentage of blood cell damage flowing across the leaflet free margin.

## 6.2 Future CFD Modeling

A CFD model of a heart valve should address several key issues specifically related to hemodynamics. Aside from pressure drops, shear stresses, flow patterns (as it pertains to thrombogenicity), and turbulence, researchers should also focus on cavitation damage in mechanical heart valves and closure dynamics. An ideal CFD model of a heart valve (both native and prosthetic) would be transient, three-dimensional, and account for fluid-structure interaction. Developing a transient model to reflect the pulsatile nature of blood flow through heart valves requires a knowledge of the hemodynamics of the entire cardiac cycle and the interaction of the valve with blood flow. Though desirable, this methodology would require a remeshing scheme for each time step and material properties of the valve (which can be difficult to define for anisotropic native heart valve leaflets) are required. The three dimensional model circumvents problems associated with the asymmetries of the aortic valve due to the sinuses, coronary ostia, eccentricity of flow, and leaftlet morphology. A drawback of three-dimensional modeling is the cost associated with increased spatial resolution and nodes required. Despite this, three-dimensional models are still desired over two-dimensional models.

Fluid flow through the sinotubular junction involves increasing Reynolds num-

ber across the valve and so CFD analysis should consider the different flow characteristics associated with the viscous sublayer and turbulent layer. As such The unsteadiness of flow should also be addressed. Particularly for mechanical heart valves, the unsteadiness is associated with the pulsatile flow, vortex shedding, and the closure of the heart valve [7].

Although this work relied on numerical solutions to the Navier-Stokes equations, the alternate method for CFD analysis based on lattice Boltzmann methods using has been used by reseachers [22]. The lattice Boltzmann methods are intrinsically Lagrangian since they model particle dynamics.

Future studies that use the same methods and modeling discussed in this work should elaborate on fluid dynamical assessment at other stages in the cardiac cycle, particularly early systole and the start of ventricular diastole (especially for the study of closure dynamics).

## 6.3 Conclusions

Despite the relative simplicity of the CFD models, the biological valve shows considerable improvement compared to the SE valve in terms of pertinent parameters such as pressure drop, velocity profiles, hemolysis generation, and turbulent kinetic energy production. Modeling at peak velocity, the biological valve produced a smaller pressure drop, less hemolysis generation, less downstream turbulent kinetic energy production, and a parabolic downstream velocity profile compared to the SE

valve at peak velocity. From a hemodynamical assessment, the biological valve is an improvement over the SE valve. Table 6.1 shows a comparison of hemodynamic characteristics.

| Valve | Pressure Drop (mmHg) | Shear Stress ($N/m^2$) | Hemolysis (%) |
|---|---|---|---|
| SE | 12.0 | 42.3 | 1.29 |
| Biological | 6.5 | 36.0 | 1.14 |

**Table 6.1: A Comparison of Hemodynamic Properties.**

One can credit the closer approximation to the native heart valve as the reason for the improvement. Improvement on the existing biological valve is primarily a question for material biocompatibility. The models did not consider a fluid-structure coupling since the focus of the study was based on the valve's influence on the local hemodynamics rather than the effects on the valve and the surrounding physiological structure. As such, the models created are sufficient since they capture the physics associated with blood flow without being too complicated with a functional fluid-structure coupling (where material properties of the valve are of equal interest compared to the fluid properties).

# Appendix A

# The Navier Stokes Equations

The fundamental equations that describe fluid flow are the Navier-Stokes equations. The Navier-Stokes equations are derived from the continuity equation and momentum conservation. Conservation of mass can be evaluated by analyzing a mass balance in an arbitrary control volume:

$$\frac{\partial \rho}{\partial t} = -\nabla \cdot (\rho \mathbf{v}) \tag{A.1}$$

where $\mathbf{v}$ is the velocity vector with components $(u, v, w)$. The LHS is the time rate of change of density and the RHS is a convective term that accounts for net mass flow across the boundary of the control volume. The previous equation is a general equation since it is valid for compressible fluids. For incompressible fluids, the equation reduces to

$$\nabla \cdot \mathbf{v} = 0 \tag{A.2}$$

Momentum conservation for viscous flow is determined by analyzing the balance

of forces acting on an arbitrary fluid element. The surface forces associated with the pressure are replaced by a general stress tensor $\sigma_{ij}$. The average of the normal stresses is set equal to the negative of the pressure and the remaining contributions of the stress tensor are due to the viscous nature of the fluid [23]. The contributions constitute a symmetric viscous stress tensor $\tau_{ij}$ such that

$$\sigma_{ij} = -P\delta_{ij} + \tau_{ij} \tag{A.3}$$

where $\delta_{ij}$ is the Kronecker delta[1] and $P$ is the pressure.

The components of the momentum equation for viscous flow can be determined by using Newton's second law on a fluid element since the rate of change of linear momentum is equal to the net force acting on the element. The surface forces acting on the fluid element depend on whether the fluid is treated as viscous or inviscid. The momentum components are given by [23]:

$$\frac{D(\rho u)}{Dt} = \rho f_x - \frac{\partial P}{\partial x} + \frac{\partial \tau_{xx}}{\partial x} + \frac{\partial \tau_{xy}}{\partial y} + \frac{\partial \tau_{xz}}{\partial z} \tag{A.4}$$

$$\frac{D(\rho v)}{Dt} = \rho f_y - \frac{\partial P}{\partial y} + \frac{\partial \tau_{xy}}{\partial x} + \frac{\partial \tau_{yy}}{\partial y} + \frac{\partial \tau_{yz}}{\partial z} \tag{A.5}$$

$$\frac{D(\rho w)}{Dt} = \rho f_z - \frac{\partial P}{\partial z} + \frac{\partial \tau_{xz}}{\partial x} + \frac{\partial \tau_{yz}}{\partial y} + \frac{\partial \tau_{zz}}{\partial z} \tag{A.6}$$

where $\mathbf{f} = (f_x, f_y, f_z)$ is the volumetric force per unit mass and the operator $D/Dt$

[1] In its tensor form, the Kronecker delta behaves similar to the identity matrix.

is the material or convected derivative [24]. The material derivative is a derivative that evaluates a quantity of interest (momentum per unit volume in this specific case) for a fluid element while moving along a trajectory in a velocity field. Due to the nature of the material derivative, it is applicable to Lagrangian descriptions (where material coordinates are the independent variables).

The components of the viscous stress tensor are related to the rates of strain and are given by [23]:

$$\tau_{xx} = -\frac{2}{3}\mu\left(\nabla \cdot \mathbf{v}\right) + 2\mu\frac{\partial u}{\partial x} \tag{A.7}$$

$$\tau_{yy} = -\frac{2}{3}\mu\left(\nabla \cdot \mathbf{v}\right) + 2\mu\frac{\partial v}{\partial y} \tag{A.8}$$

$$\tau_{zz} = -\frac{2}{3}\mu\left(\nabla \cdot \mathbf{v}\right) + 2\mu\frac{\partial w}{\partial z} \tag{A.9}$$

$$\tau_{xy} = \mu\left(\frac{\partial u}{\partial y} + \frac{\partial v}{\partial x}\right) \tag{A.10}$$

$$\tau_{xz} = \mu\left(\frac{\partial u}{\partial z} + \frac{\partial w}{\partial x}\right) \tag{A.11}$$

$$\tau_{yz} = \mu\left(\frac{\partial v}{\partial z} + \frac{\partial w}{\partial y}\right) \tag{A.12}$$

Substituting the shear stress terms into the momentum component equations and rearranging results in the Navier-Stokes equations:

$$\rho\frac{Du}{Dt} = \rho f_x - \frac{\partial P}{\partial x} - \frac{2}{3}\frac{\partial\left(\mu\nabla\cdot\mathbf{v}\right)}{\partial x} + 2\frac{\partial}{\partial x}\left(\mu\frac{\partial u}{\partial x}\right) + \frac{\partial}{\partial y}\left[\mu\left(\frac{\partial u}{\partial y} + \frac{\partial v}{\partial x}\right)\right] + \frac{\partial}{\partial z}\left[\mu\left(\frac{\partial u}{\partial z} + \frac{\partial w}{\partial x}\right)\right] \tag{A.13}$$

$$\rho\frac{Dv}{Dt} = \rho f_y - \frac{\partial P}{\partial y} - \frac{2}{3}\frac{\partial\left(\mu\nabla\cdot\mathbf{v}\right)}{\partial y} + \frac{\partial}{\partial x}\left[\mu\left(\frac{\partial u}{\partial y} + \frac{\partial v}{\partial x}\right)\right] + 2\frac{\partial}{\partial y}\left(\mu\frac{\partial v}{\partial y}\right) + \frac{\partial}{\partial z}\left[\mu\left(\frac{\partial v}{\partial z} + \frac{\partial w}{\partial y}\right)\right] \tag{A.14}$$

$$\rho\frac{Dw}{Dt} = \rho f_z - \frac{\partial P}{\partial z} - \frac{2}{3}\frac{\partial\left(\mu\nabla\cdot\mathbf{v}\right)}{\partial z} + \frac{\partial}{\partial x}\left[\mu\left(\frac{\partial u}{\partial z} + \frac{\partial w}{\partial x}\right)\right] + \frac{\partial}{\partial y}\left[\mu\left(\frac{\partial v}{\partial z} + \frac{\partial w}{\partial y}\right)\right] + 2\frac{\partial}{\partial z}\left(\mu\frac{\partial w}{\partial z}\right) \tag{A.15}$$

# Bibliography


[1] Marieb, E. (1992). *Human Anatomy and Physiology (2nd)*. Redwood City, CA: BC Publishing Company, Inc.

[2] Rohen, Yokochi (1993). *Color Atlas of Anatomy: A Photographic Study of the Human Body (3rd)*. Tokyo, Japan: Igaku-Shoin Ltd.

[3] Anderson, R.H. (2007). *The Surgical Anatomy of the Aortic Root*. Multimedia Manual of Cardiothoracic Surgery. doi:10.1510/mmcts.2006.002527.

[4] Waite, Fine (2007). *Applied Biofluid Mechanics*. New York, NY: McGraw-Hill.

[5] Christie, G. (1992). *Computer Modelling of Bioprosthetic Heart Valves*. European Journal of Cardiothoracic Surgery, 6, S95-S101.

[6] Starr, Haydar, Hovaguimian, et al. (1997) *Valve Repair for Aortic Insufficiency: Surgical Classification and Techniques*. European Journal of Cardiothoracic Surgery, 11, 258-265.

[7] He, Z. et al. (2004). *Fluid Mechanics of Heart Valves*. Annual Review of Biomedical Engineering, 6, 331-362.

[8] Martinez, R., et al. (2010) *Transcatheter Aortic Valve Implantation*. Cardiology Clinics, 28, 155-168, doi:10.1016/j.ccl.2009.09.002.

[9] Borrero, Cure, Fabre, et al. (2003). *Mechanics of Prosthetic Heart Valves*. Applications of Engineering Mechanics in Medicine.

[10] Bronzino, JD, ed. (1995). *The Biomedical Engineering Handbook*. Boca Raton: CRC Press. 2nd ed.

[11] Travis, B.R. 2000. Fluid Dynamics of Prosthetic Valves. *The Practice of Clinical Echocardiography*,ed. CM Otto. Philadelphia, PA: WB Saunders. 2nd ed.

[12] Merryman, Sacks, Schmidt (2009) *On the Biomechanics of Heart Valve Function*. Journal of Biomechanics, 42, 1804-1824.

[13] Li, John (2004). *Dynamics of the Vascular System*. Toh Tuck Link, Singapore: World Scientific Publishing Co.

[14] Sankar, Lee (2009). *Mathematical Modeling Of Pulsatile Flow of Non-Newtonian Fluid in Stenosed Arteries* . Communications in Nonlinear Sciences and Numerical Simulations, 14, 2971-2981.

[15] Kreith, F, ed. (1999). Fluid Mechanics. *The Mechanical Engineering Handbook*. Boca Raton: CRC Press.

[16] Gorlin, Gorlin (1957). *Hydraulic Formula for Calculation of the Area of the Stenotic Mitral Valve, Other Cardiac Valves, and Central Circulatory Shunts*. American Heart Journal, 41, 1-29.

[17] Cengel, Turner (2005). *Fundamentals of Thermal-Fluid Sciences (2nd)*. New York, NY: McGraw-Hill.

[18] CFD-ACE+ V2007.2 Modules Manual V1. Published by ESI CFD Inc.

[19] Launder, Spaulding (1974). *The Numerical Computation of Turbulent Flows*. Computer Methods in Applied Mechanics and Engineering, 3, 269-289.

[20] Lansac, E., et al. (2002). *A Four-Dimensional Study of the Aortic Root Dynamics*. European Journal of Cardiothoracic Surgery, 22, 497-503.

[21] CFD-GEOM V2008.2 User Manual. Published by ESI CFD Inc.

[22] Krafczyk M, Cerrolaza M, et. al. (1998). *Analysis of 3D Transient Blood Flow Passing Through An Artificial Aortic Valve by Lattice-Boltzmann Methods*. J. Biomech. 31:453-462.

[23] Fletcher, C. (2003). *Computational Techniques for Fluid Dynamics Vol. 2 (2nd)*. Berlin, Germany: Springer-Verlag.

[24] Spencer, A. (1980). *Continuum Mechanics*. Mineola, New York: Dover Publications, Inc.